AD-A094 774 AIR FORCE INST OF TECH WRIGHT-PATTERSON AFB OH SCHOO--ETC F/G 6/16
A VISCOELASTIC FINITE ELEMENT MODEL OF THE HUMAN INTERVERTEBRAL--ETC(U)
DEC 80 R L HINRICHSEN
UNCLASSIFIED AFIT/GAE/AA/80D-11 NL

1 OF 2
AD A094774

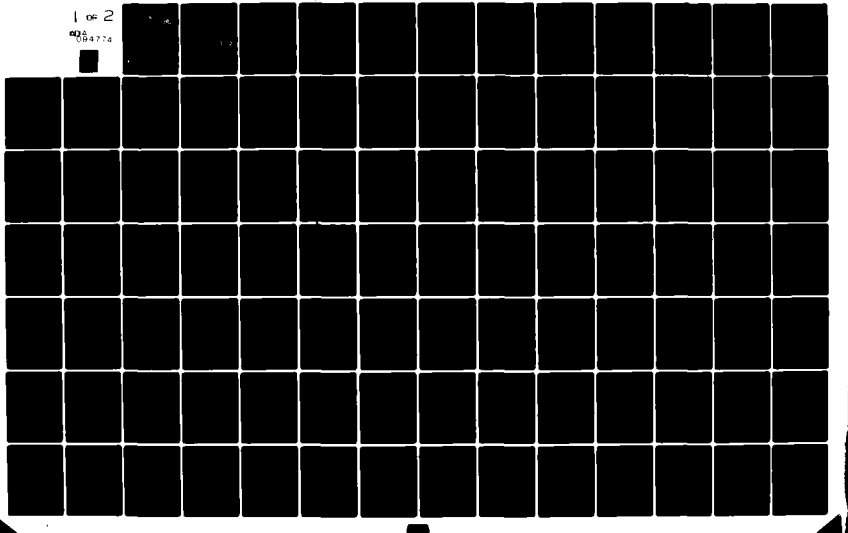

AD A094774

LEVEL II

DTIC FILE COPY

DEPARTMENT OF THE AIR FORCE

AIR UNIVERSITY (ATC)

AIR FORCE INSTITUTE OF TECHNOLOGY

Wright-Patterson Air Force Base, Ohio

14 AFIT/GAE/AA/80D-11

23 JAN 1981

APPROVED FOR PUBLIC RELEASE AFR 190-17.

Laurel A. Lampela

LAUREL A. LAMPELA, 2Lt, USAF
Deputy Director, Public Affairs
Air Force Institute of Technology (ATC)
Wright Patterson AFB, OH 45433

Accession For	
NTIS GRA&I	✓
DTIC TAB	
Unannounced	
Justification	
By	
Distribution/	
Availability Codes	
Dist	Avail and/or Special
A	

DTIC ELECTE FEB 10 1981 S D F

A VISCOELASTIC FINITE ELEMENT MODEL OF THE HUMAN INTERVERTEBRAL JOINT.

THESIS

AFIT/GAE/AA/80D-11 Ronald L. Hinrichsen

Captain USAF

Approved for public release; distribution unlimited

AFIT/GAE/AA/80D-11

A VISCOELASTIC FINITE ELEMENT MODEL OF THE HUMAN INTERVERTEBRAL JOINT

THESIS

Presented to the Faculty of the School of Engineering
of the Air Force Institute of Technology
Air University
in Partial fulfillment of the
Requirements for the Degree of
Master of Science

by

Ronald L. Hinrichsen, B.S.
Capt USAF
Graduate Aeronautical Engineering

December 1980

ACKNOWLEDGEMENTS

I would like to express my gratitude to Professor A.N. Palazotto for his patience, technical guidance, and encouragement during the course of this study. Thanks go to Dr. T.D. Hinnerichs for his helpful suggestions and guidance in applying the computer techniques presented herein. A special thanks is also extended to Capt. A.J. Nestle and the staff of the Air Force Aerospace Medical Research Laboratory who sponsored the study and provided the necessary computer resources.

My most sincere gratitude is extended to my wife and family for their love and support, without which this study could have been neither undertaken nor completed.

Ronald L. Hinrichsen

CONTENTS

List of Figures

List of Symbols

$\Delta( )$	Small change in ( )
$(\dot{})$	Time rate of change of ( )
a	Outer radius of a cylinder
[A]	Matrix of Poisson's ratio terms
b	Inner radius of a cylinder
d/dt	Time derivative
D	Time differential operator
e	Spherical strain
e	Deviatoric strain tensor
E	Young's modulus
G	Elastic shear modulus
h	Height
K	Elastic bulk modulus
k	Summation index
Kp	Kilopond
m	Summation limit
n	Summation limit
p	Polynomial operator coefficient
P	Differential operator
$\mathcal{P}$	Polynomial operator
q	Differential operator coefficient
Q	Differential operator
$\mathcal{Q}$	Polynomial operator
r	Radius radial coordinate direction
s	Spherical stress

$\hat{s}$	Deviatoric stress
ν	Transform variable
Sqcm	Square centimeter
t	Time
u	Displacement
z	Axial coordinate direction
η	Dashpot constant
ϵ	Strain
$\bar{\epsilon}$	Transform strain
ν	Poisson's ratio
σ	Stress
$\bar{\sigma}$	Transform stress
θ	Tangential coordinate direction

ABSTRACT

The combined mechanical stresses on aircrewmen have become increasingly acute as technological developments extend the flight envelopes of our high performance aircraft. Limitations on the design of this type of aircraft are frequently dictated by human tolerance. The concept of an analytical model to evaluate the biomechanical response of the human intervertebral joint, under the influence of long term axial compressive loading, is important in assessing the load carrying capability of normal and diseased vertebral segments.

It has been experimentally demonstrated that healthy intervertebral joints are composed of materials which exhibit creep characteristics. This investigation is significant because it presents a study of the time dependant behavior involved. An axisymmetric finite element model is employed which incorporates a linear viscoelastic constitutive relation for the intervertebral disc. Viscoelastic material constants are found by matching one-dimensional experimental data with the two-dimensional model. Results are presented depicting displacement profiles and stress redistributions occurring as a consequence of the inclusion of these viscoelastic parameters which, for the first time, simulate the actual human response to high compressive loads over a specific time span.

CHAPTER 1

INTRODUCTION

1.1 Background

An understanding of the mechanics of the intervertebral joint is of interest to researchers in many areas; ranging from problems encountered during pilot ejections to those associated with the selection of suitable disc replacement materials. At the present time, however, even some of the salient features of the joint's mechanical behavior are poorly understood . This is a consequence of the difficulties in determining in-vivo mechanical properties and constructing a realistic analytical model. (Belytschko et.al.(3))

Research into the material properties of vertebral bone has been performed by Galante et.al.(10), Rockoff et.al.(20), and McElhaney (17). The use of the finite

element method to successfully model the vertebral body has been demonstrated by Balasulramanian et.al.(2) and Hakim et.al.(11).

Brown et.al.(6), Nachemson (18), Hirsh (14), and Rolander (21) carried out experiments to determine the static force deflection properties of the intervertebral disc subjected to axial loading. Belytschko et.al.(4) and Spilker (23) employed an axisymmetric finite element model to study the time independant behavior of the intervertebral disc.

Meanwhile, Kazarian (15) reported creep characteristics for intervertebral joints subjected to constant axial loads, and Kazarian et.al.(16) illustrated that the response could be adequately modelled with a three-parameter viscoelastic solid. Using a one-dimensional classical approach, Burns (7) derived the material constants for these three-parameter solids.

1.2 Purpose

As a natural extension of the work which has been done to date, this thesis was undertaken to include in the model of the intervertebral joint, not only the geometric irregularities and material inhomogeneity, but the viscoelastic creep response previously noted. The purpose in doing so was to determine the applicability of using the one-dimensional parameters derived by Kazarian et.al.(16)

and Burns (7) in a three-dimensional model. Secondly, to observe the influence of a creeping disc on the displacement profiles and stress redistributions within the vertebral body.

1.3 Anatomy (4)

The human vertebral column is a segmented structure of 24 mobile vertebrae separated by intervertebral discs. Each vertebra consists of a body and a set of posterior elements. The center of the vertebral body is composed of soft trabecular bone, and is encased circumferentially by a thin shell of relatively hard cortical bone. The upper and lower surfaces of the body, which are also thin plates of cortical bone, constitute the bony end-plates.

The intervertebral disc is a rather complex entity containing both solid and fluid material. Exterior to the disc proper are two ligaments: the anterior longitudinal ligament and the posterior longitudinal ligament. The posterior ligament is attached dorsally, while the anterior ligament is attached ventrally, to the disc.

The combination of two vertebral bodies with their intermediate ligaments and disc is what constitutes the intervertebral joint. During axial loading the disc appears to be the primary load-carrying structure between vertebrae (14), (18),(21), and thus any ligament restraint is removed in order to focus entirely upon the disc interaction. (See Fig (1.1) and (1.2))

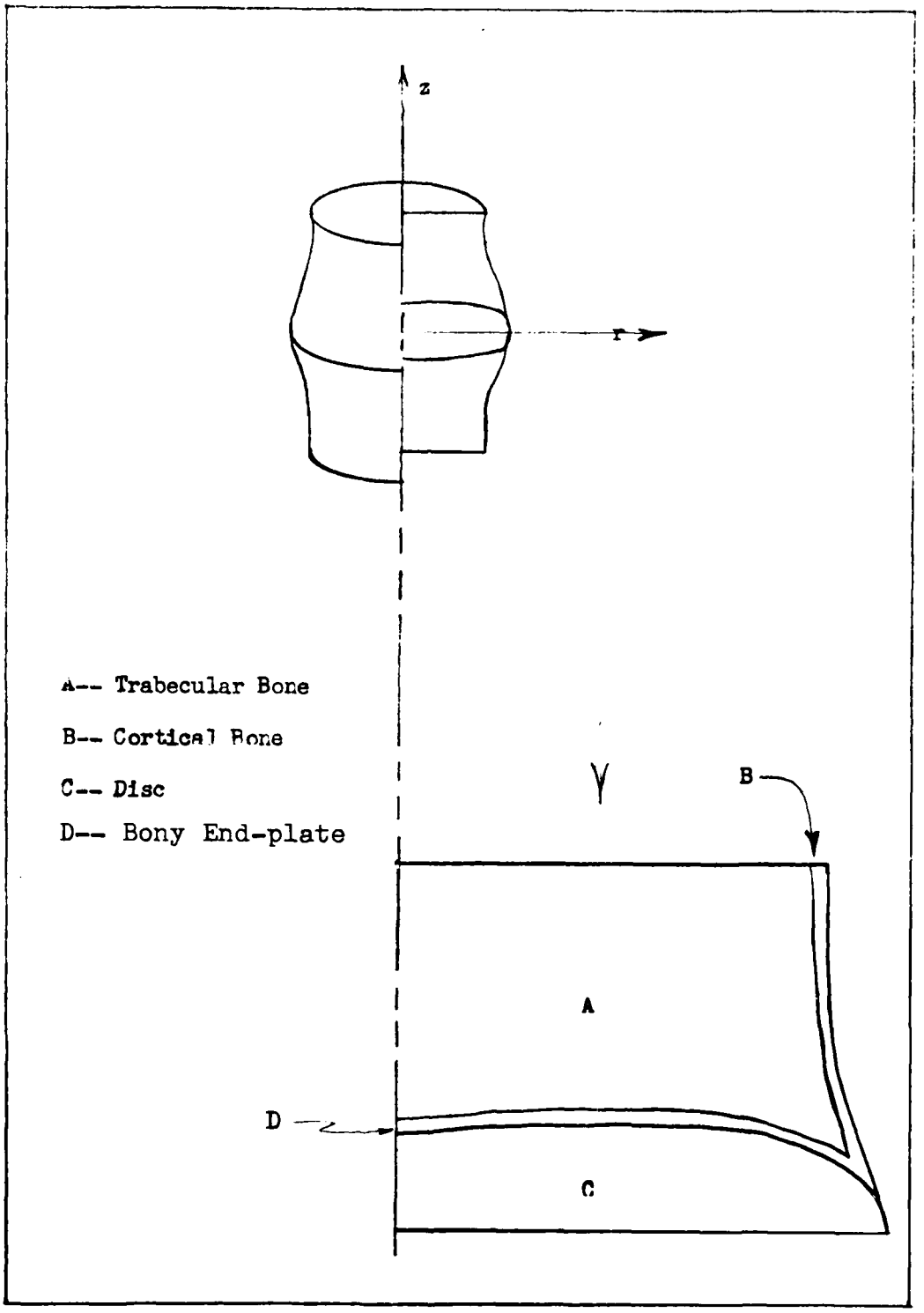

Figure 1.1 Truncated Intervertebral Joint

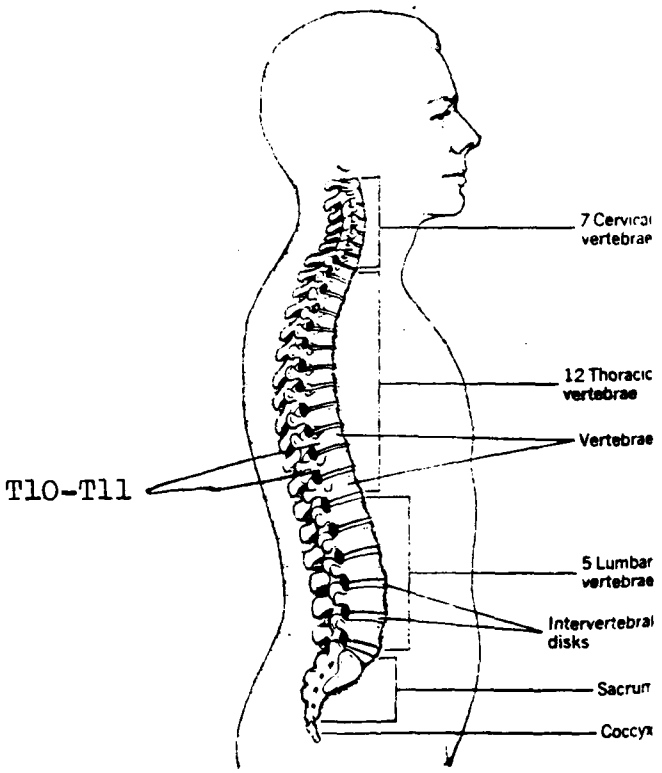

Figure 1.2 The Human Spine

1.4 General Approach and Assumptions

Initially, analytical techniques were investigated as an approach to modelling the joint. This investigation revealed the joint to be of such complexity that classical methods could not be applied. The finite element method, however, was found to be capable of handling the complexity, and therefore was pursued.

An existing plane-stress, plane-strain finite element program written by Hinnerichs (12) was modified to account for material viscoelasticity and inhomogeneity. Since the intervertebral joint was idealized as a body of revolution, the program was further altered to accommodate axisymmetric structures. These modifications were validated before the program was applied to the problem at hand.

In addition to the assumption of axisymmetry, it was also assumed that the intervertebral joint was symmetric with respect to the centerline of the disc. It was further assumed that the observed creep was a quasi-static phenomenon; in which case, the inertia of the structure was neglected. Kazarian (15) showed viscoelastic creep of the joint to be dependant on the presence of the disc. That is, the vertebral body alone did not exhibit creep when subjected to a constant axial load. Therefore, it was assumed that the trabecular and compacted bone of the vertebral body were linear elastic materials, whereas the disc was idealized as a homogeneous isotropic linear

viscoelastic substance. In other words, all of the viscoelasticity of the joint was attributed to the disc.

Based on these assumptions, a T10-T11 spinal segment (test I.D. 65 Kazarian et.al.(16)) was discretized and studied. (See Fig 1.2 for their relative location in the spine)

CHAPTER 2

LINEAR VISCOELASTIC THEORY

The classical theory of elasticity deals with the mechanical properties of elastic solids, for which, according to Hooke's law, stress is always directly proportional to strain in small deformations, but independant of strain rate Saada(22). The classical theory of hydrodynamics deals with properties of viscous fluids, for which, according to Newton's law, stress is always directly proportional to the rate of strain, but independant of the strain itself.

The classical theories of elasticity and hydrodynamics are idealizations, and many materials cannot be adequately modelled by one or the other of them. For instance, a material which is not quite solid does not maintain a constant deformation under constant stress, but slowly deforms with time. When such a material is constrained at constant deformation, the stress required to hold it

gradually diminishes or relaxes. A material which is not quite liquid may, while flowing under constant stress, store some of the energy input, instead of dissipating it. It may recover all of its deformation when the stress is removed. Materials which exhibit such behavior are identified as viscoelastic and can be adequately modelled by combining the classical theories of elasticity and hydrodynamics.

2.1 Classical Viscoelastic Theory

An extensive study of the viscoelastic theory has been performed by a number of researchers. Principal results are summarized in texts by Bland(5), Christensen(8), and Flugge(9). A brief discussion of the theory is presented here as a background for the reader.

2.1.1 One-Dimensional Theory (9)

The building blocks or discrete elements of linear viscoelastic theory are the spring and the dashpot. Various combinations of these elements serve to model the many different types of viscoelastic materials. To understand the combinations of these elements one must investigate their individual characteristics.

Consider a helical spring which obeys Hooke's law. Its constitutive equation may be written as

$$\sigma = E\epsilon \tag{2-1}$$

where σ is the stress, ϵ the strain, and E the Modulus of elasticity. Similarly for the dashpot

$$\sigma = \eta\dot{\epsilon} \tag{2-2}$$

where η is the dashpot constant and ($\dot{}$) denotes time differentiation.

Perhaps the simplest combination of these elements is the Maxwell fluid (Fig 2.1) in which the elements are placed in series.

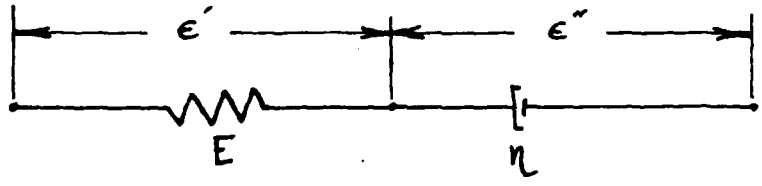

Figure (2.1)

To derive the constitutive equation for this model, the equations of the two elements are written

$$\sigma = E\epsilon' \tag{2-3}$$

and

$$\sigma = \eta\dot{\epsilon}'' \quad \Longrightarrow \quad \dot{\epsilon}'' = \frac{\sigma}{\eta} \tag{2-4}$$

It is required that the total strain be the combination of the two elemental strains,

$$\epsilon = \epsilon' + \epsilon'' \qquad (2\text{-}5)$$

Eqs 2-3 and 2-5 are differentiated with respect to time and substitutions are made for $\dot{\epsilon}'$ and $\dot{\epsilon}''$. Thus the constitutive equation is derived

$$\dot{\epsilon} = \frac{\dot{\sigma}}{E} + \frac{\sigma}{\eta} \qquad (2\text{-}6)$$

Written in standard form the equation is

$$\sigma + p_1 \dot{\sigma} = q_1 \dot{\epsilon} \qquad (2\text{-}7)$$

where (in this case) $p_1 = \frac{\eta}{E}$ and $q_1 = \eta$.

Another combination of these elements is the Kelvin solid (Fig. 2.2) in which the elements are placed parallel to one another.

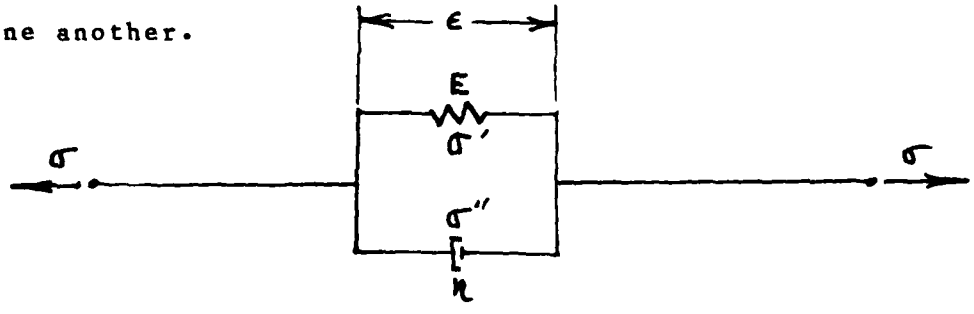

Figure (2.2)

The derivation of the constitutive equation for the Kelvin solid proceeds in a manner similar to the Maxwell fluid. In this case it is required that the total stress be equal to the combination of the two stresses

$$\sigma = \sigma' + \sigma'' \qquad (2\text{-}8)$$

The constitutive equation is found by substituting in for σ'

and σ''.

$$\sigma = E\epsilon + \eta\dot{\epsilon} \tag{2-9}$$

which is written in standard form

$$\sigma = q_0\epsilon + q_1\dot{\epsilon} \tag{2-10}$$

where (in this case) $q_0 = E$ and $q_1 = \eta$.

More complicated models are built by systematically combining the discrete elements with Kelvin solids and/or Maxwell fluids. The constitutive equation for any such model has the form

$$p_0\sigma + p_1\dot{\sigma} + p_2\ddot{\sigma} + \cdots = q_0\epsilon + q_1\dot{\epsilon} + q_2\ddot{\epsilon} + \cdots \tag{2-11}$$

Or

$$\sum_{k=0}^{m} p_k \frac{d^k\sigma}{dt^k} = \sum_{k=0}^{n} q_k \frac{d^k\epsilon}{dt^k} \tag{2-12}$$

If the differential operators are defined

$$P = \sum_{k=0}^{m} p_k \frac{d^k}{dt^k} \quad ; \quad Q = \sum_{k=0}^{n} q_k \frac{d^k}{dt^k} \tag{2-13}$$

then eq 2-12 can be written in the form

$$P\sigma = Q\epsilon \tag{2-14}$$

which resembles Hooke's law.

The solution of Eq 2-14 for σ or ϵ as a function of time is not a trivial problem. Perhaps the most universally applied solution process is to subject the equation to the Laplace transformation which results in an algebraic relation between the transforms $\bar{\sigma}$ and $\bar{\epsilon}$ of stress and strain

$$\sum_{k=0}^{m} p_k s^k \bar{\sigma} = \sum_{k=0}^{n} q_k s^k \bar{\epsilon} \qquad (2\text{-}15)$$

where s is the transform variable.

If the polynomial operators are defined

$$P = \sum_{k=0}^{m} p_k s^k \quad ; \quad Q = \sum_{k=0}^{n} q_k s^k \qquad (2\text{-}16)$$

then Eq 2-15 becomes

$$P\bar{\sigma} = Q\bar{\epsilon} \qquad (2\text{-}17)$$

Again, note the similarity to Hooke's law.

2.1.2 Three-Dimensional Theory (9)

To this point in the presentation, consideration has been given only to uniaxial states of stress and strain and an expression for the constitutive equation of a one-dimensional linear viscoelastic material has been derived. Next, a multiaxial state of stress is considered and a general constitutive equation for a three-dimensional

viscoelastic material is found. In order to do this, the elastic constitutive equations must first be presented.

In elasticity, the state of stress and strain in a material can be described with second-order cartesian tensors σ_{ij} and ϵ_{ij} (22). If the material is isotropic, then only two material constants are required to express the constitutive equation. These constants are Young's modulus and Poisson's ratio. The constitutive equation may be expressed

$$\{\epsilon\} = \frac{1}{E}[A]\{\sigma\} \qquad (2\text{-}18)$$

where [A] is dependant on Poisson's ratio ν.

Another way of expressing this relationship is by separating the stress tensor into its spherical and deviatoric components and writing

$$s = 3Ke \qquad (2\text{-}19)$$

$$\hat{s} = 2G\hat{e} \qquad (2\text{-}20)$$

where K and G are the bulk and shear moduli , s and e the spherical stress and strain, $\hat{s}$ and $\hat{e}$ the deviatoric stress and strain respectively. If an elastic material were subjected to a hydrostatic state of stress then there would be a volume change but no change in shape. In other words, the spherical components (Eq 2-19) would be affected, but

the deviatoric components (Eq 2-20) would not.

Similarly, if a viscoelastic material is isotropic, a hydrostatic stress must produce a volume change and no distortion. The quantities s and e must therefore be connected by a relation such as eq 2-14, and should be written

$$\sum_{k=0}^{m''} p_k'' \frac{d^k s}{dt^k} = \sum_{k=0}^{n''} q_k'' \frac{d^k e}{dt^k} \qquad (2\text{-}21)$$

or

$$P'' s = Q'' e \qquad (2\text{-}22)$$

Similarly for the shear components

$$\sum_{k=0}^{m'} p_k' \frac{d^k \hat{s}}{dt^k} = \sum_{k=0}^{n'} q_k' \frac{d^k \hat{e}}{dt^k} \qquad (2\text{-}23)$$

Or

$$P' \hat{s} = Q' \hat{e} \qquad (2\text{-}24)$$

The four operators P', Q', P'', Q'', which describe the viscoelastic behavior of the material are entirely independant of one another.

The elastic solid is a limiting case of the viscoelastic material. It is seen that in this case the four operators are simply mulitplicative constants

$$P'' = 1 \, , \; Q'' = 3K \, , \; P' = 1 \, , \; Q' = 2G \tag{2-25}$$

In an elastic solid under constant load, nothing depends on time. In a viscoelastic material, all stresses, strains, and displacements which are material dependant are also time dependant. If the Laplace transformation is applied to eqs 2-22 and 2-24 they become

$$\Theta'' \bar{s} = 2'' \bar{e} \tag{2-26}$$

and

$$\Theta' \hat{\bar{s}} = 2' \hat{\bar{e}} \tag{2-27}$$

These are algebraic relations which become identical with their elastic counterparts (Eqs 2-19 and 2-20) if the following substitutions are made:

$$3K \rightarrow \frac{2''}{\Theta''} \, , \quad 2G \rightarrow \frac{2'}{\Theta'} \tag{2-28}$$

This leads to a most general correspondence principle: (5) If the solution of an elastic problem is known, the Laplace transformation of the solution to the corresponding viscoelastic problem may be found by replacing the elastic constants K and G by quotients of polynomial operators and the actual loads by their Laplace transforms.

In most cases the solutions of elastic problems are not

written in terms of K and G, but rather in terms of E and ν. The elastic relations between E, ν, K and G are (22)

$$E = \frac{9KG}{3K+G} \quad , \quad \nu = \frac{3K-2G}{6K+2G} \tag{2-29}$$

If the corresponding viscoelastic polynomial operators for K and G are substituted into Eq 2-29, the following expressions are obtained:

$$E = \frac{3\mathcal{Q}'\mathcal{Q}''}{2\mathcal{Q}'\mathcal{Q}'' + \mathcal{Q}'\mathcal{Q}''} \tag{2-30}$$

and

$$\nu = \frac{\mathcal{Q}'\mathcal{Q}'' - \mathcal{Q}'\mathcal{Q}''}{2\mathcal{Q}'\mathcal{Q}'' + \mathcal{Q}'\mathcal{Q}''} \tag{2-31}$$

This correspondence principle is of sweeping generality, but it does have its limitations. It requires that one has closed form solutions to the elastic problem, which, for nonhomogeneous structures of complicated geometry, are unattainable.

The viscoelastic creep of the human intervertebral joint is such a problem. Thus, the classical viscoelastic correspondence principle must be abandoned as a solution technique and another method must be tried, namely the finite element method.

2.2 The Finite Element Method

Numerous authors have presented works which detail the solution of linear and nonlinear elastic problems by the finite element method. Among them are Bathe et.al.(3), Oden(19), and Zienkiewicz(25). Appendix A gives a brief overview of its application to an elastic, axi-symmetric structure under initial strain. The solution of the viscoelastic problem by this technique is based on the assumption that the material of the structure can be adequately modelled by a finite number of Kelvin solids or Maxwell fluids coupled with an elastic spring [Adey et.al.(1), White(24), Zienkiewicz et.al.(26)]. This assumption is satisfied as long as the coefficient of the zeroth-order derivative of eqns 2-12, 2-21, or 2-23 is nonzero.

2.2.1 One-Dimensional Problems (26)

For simplicity of presentation, it is assumed that the structure in question is one-dimensional and can be modelled as a three-parameter solid, ie. One Kelvin solid coupled with an elastic spring. The instantaneous elastic deformation is dependant only on the spring and therefore can be separated from the creep deformation and solved by the finite element method. The Kelvin solid (Fig 2.2) whose constitutive relationship is given by eqn 2-9, is next

considered. This equation may be rewritten

$$\dot{\epsilon}_c = \frac{1}{\eta}\sigma - \frac{E}{\eta}\epsilon_c \qquad (2\text{-}32)$$

which shows that the creep strain rate is a function of current stress level and total accumulated creep strain. This expression is integrated by Euler's time derivative method [Hornbeck(13)] to yield

$$\Delta\epsilon_c = \frac{1}{\eta}(\sigma - E\epsilon_c)\Delta t \qquad (2\text{-}33)$$

The quantity $\Delta\epsilon_c$ represents the change in strain due to creep at the end of a small time interval . This can be considered as an initial strain imposed. The elastic problem is solved again for a new stress system. Time is incremented and the whole process is repeated in this incremental fashion until a maximum time is reached. The foregoing algorithm is more completely discussed in Appendix A.

In general, for any viscoelastic material model, eqn 2-14 must be employed, which can be rewritten

$$\epsilon_c = \frac{P}{Q}\sigma \qquad (2\text{-}34)$$

Advantage is taken of the similarity of this equation with Hooke's law. That is, for uniaxial conditions, the quantity $1/E$ of a simple elastic case is replaced by the operator P/Q for the viscoelastic case.

2.2.2 Three-Dimensional Problems (26)

To generalize this technique to the multiaxial case an appeal is made to the multiaxial elastic relationships 2-19 and 2-20 as well as the similar viscoelastic relationships 2-22 and 2-24.

From these relations it can be seen that $1/3K$ and $1/2G$ of the simple elastic case are replaced by the operators P''/Q'' and P'/Q' for the viscoelastic case.

Again for simplicity of presentation, it is assumed that the material is elastic in volume change and a three parameter solid in distortion. With these assumptions, the operators become

$$1/3K = P''/Q'' = 1/3K \tag{2-35}$$

and

$$1/2G = P'/Q' = q + 1/(q_0 + q_1 D) \tag{2-36}$$

where

$$D = d/dt \tag{2-37}$$

As in the one-dimensional case it is necessary to separate the elastic terms from the viscoelastic creep terms. This is done simply by noting which terms are time

dependant and which are not. The volume change is assumed to be all elastic so it may easily be written

$$1/3K = (1/3K)_e + (0)_c \qquad (2\text{-}38)$$

where the subscripts "e" and "c" denote elastic and creep respectively. The elastic part is given by

$$(1/3K)_e = 1/3K \qquad (2\text{-}39)$$

and the creep part is given by

$$(1/3K)_c = 0 \qquad (2\text{-}40)$$

From the distortion equation the parts are separated similarly. The elastic part is

$$(1/2G)_e = q \qquad (2\text{-}41)$$

and the creep part is

$$(1/2G)_c = 1/(q_0 + q_1 D) \qquad (2\text{-}42)$$

Now, since it is desired that these relations be applied to the finite element method, the values ν and Elastic modulus must be solved for. In order to do this, the elastic parts are grouped together

$$(1/3K)_e = 1/3K \quad ; \quad (1/2G)_e = q \qquad (2\text{-}43)$$

Elastic modulus and ν are found using eqn 2-29.

$$(E)_e = \frac{9K}{6Kq + 1} \tag{2-44}$$

and

$$(\nu)_e = \frac{3Kq - 1}{6Kq + 1} \tag{2-45}$$

the creep parts are grouped together

$$(1/3K)_c = 0 \quad ; \quad (1/2G)_c = 1/(q_0 + q_1 D) \tag{2-46}$$

and solved for

$$(\nu)_c = 1/2 \quad ; \quad (1/E)_c = 2/3\left(1/q_0 + q_1 D\right) \tag{2-47}$$

In order to use these quantities in the finite element method eqn 2-18 must be returned to. For the elastic part the values of ν_e and E_e are substituted and the instantaneous elastic deformation is solved using the finite element method. For the creep part, the values for ν_e and E_e are substituted to obtain

$$\{\epsilon_c\} = 2/3\left(1/q_0 + q_1 D\right)[A]\{\sigma\} \tag{2-48}$$

which is rewritten

$$\{\dot{\epsilon}_c\} = 2/3\,[A]\{\sigma\} - q_0/q_1\,\{\epsilon_c\} \tag{2-49}$$

This equation is integrated by Euler's method to yield

$$\{\Delta\epsilon_c\} = \frac{\Delta t}{q_1}\left[\tfrac{2}{3}[A]\{\sigma\} - q_0\{\epsilon_c\}\right] \qquad (2\text{-}50)$$

Again, as in the uniaxial case, the $\{\Delta\epsilon_c\}$ becomes an initial strain imposed and the finite element method proceeds similarly. (If the reader is specifically interested in the use of Eq 2-50 within the finite element formulation, Appendix A may be consulted.)

CHAPTER 3

PROGRAM VALIDATION

As was mentioned in the introduction, numerous changes were made to an existing finite element program. The first step following these changes was to test the program against some known exact viscoelastic solutions.

3.1 One-Dimensional Axial Rod

The first test was conducted to demonstrate the validity of the program's application to a simple one-dimensional problem. A homogeneous circular rod having three-parameter viscoelasticity was subjected to a constant axial load. Fig. (3.1) shows the rod and the finite element mesh used to model it, while a comparison of the displacements with the exact solution is presented in Fig. (3.2). The depicted solution was obtained by using an

initial timestep of ten seconds which varied to a value of 47 seconds at the conclusion of the problem. The approximate values were within 1% of the exact solution.

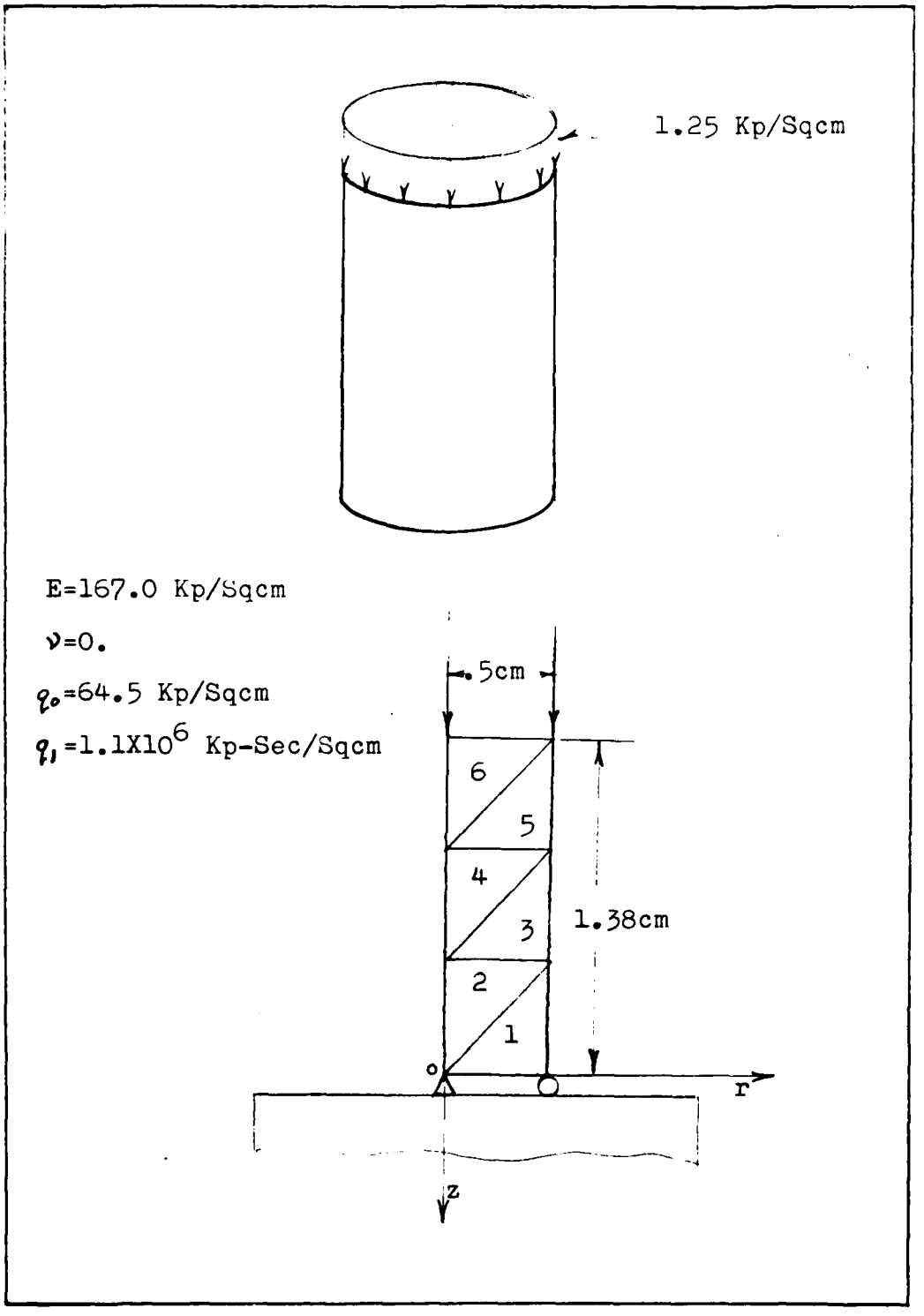

Figure 3.1 Homogeneous Circular Rod

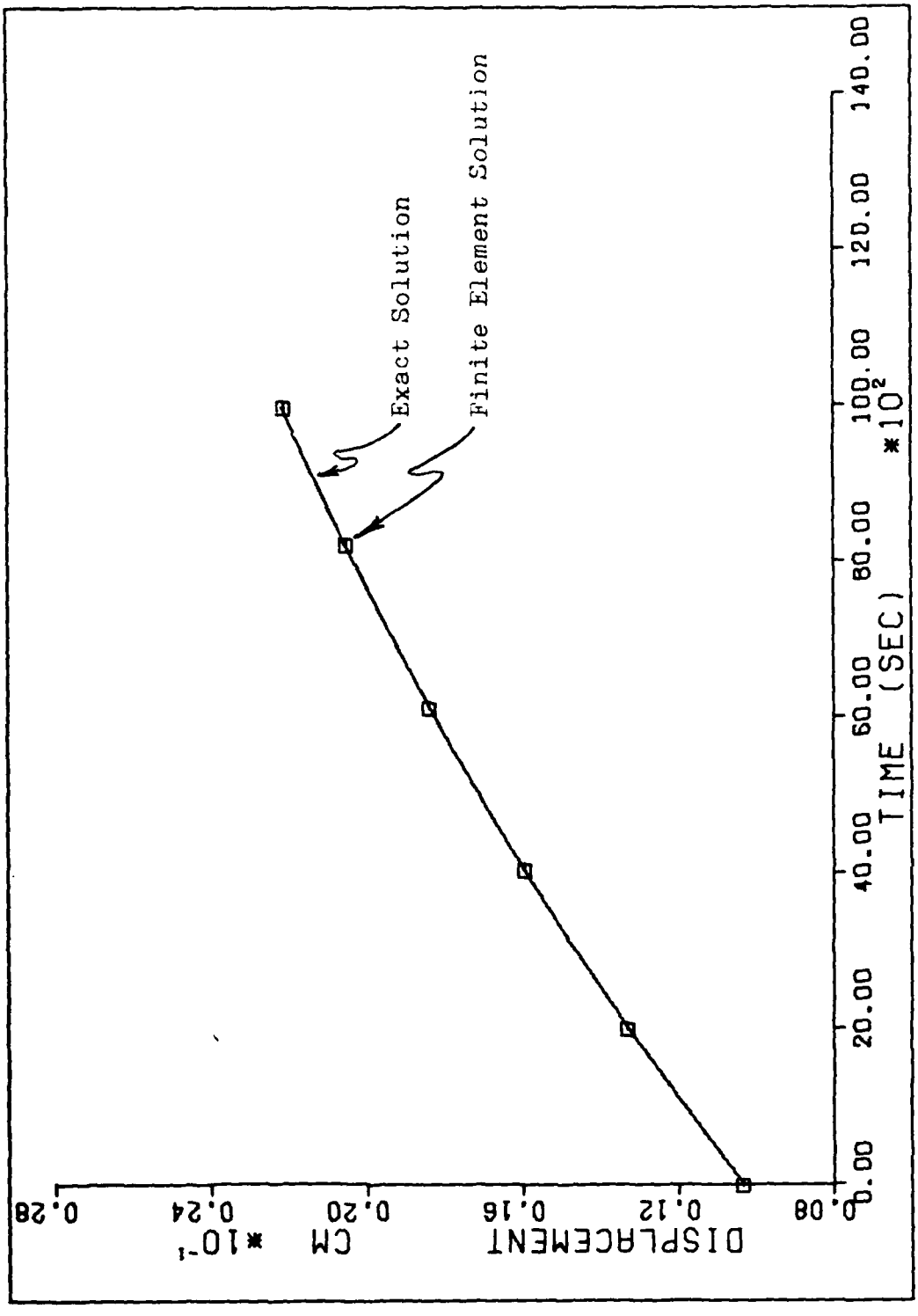

Figure 3.2 Axial Rod Displacement vs Time

3.2 Thick-Walled Cylinder Subjected to Internal Pressure

Whereas the first example tested the program for accuracy in handling a very simple structure under an axial load, the second example was designed to test the method on a relatively complex problem under radial loading. The thick-walled cylinder problem was chosen, because an exact solution could be derived using the general correspondence principle and it also provided the desired complexity. Fig. (3.4) shows the geometry and boundary conditions of the problem.

3.2.1 Exact Solution

In order to apply the general correspondence principle, the elastic solution was needed. The plane-strain assumption was made which led to the following elastic solution for the problem:

$$\sigma_r = \frac{pb^2}{a^2-b^2}\left(1-\frac{a^2}{r^2}\right);\ \sigma_\theta = \frac{pb^2}{a^2-b^2}\left(1+\frac{a^2}{r^2}\right);\ \sigma_z = \frac{2\nu pb^2}{a^2-b^2} \qquad (3\text{-}1)$$

$$u_r = \frac{(1+\nu)pb^2}{E(a^2-b^2)}\left[(1-2\nu)r + \frac{a^2}{r}\right] \qquad (3\text{-}2)$$

It was noted that σ_r and σ_θ are independant of the material constants, and therefore, in the viscoelastic problem these stresses should be time invariant. The

displacement u_r and the other stress σ_θ, however, are material dependant and therefore should be time dependant in the viscoelastic problem. These quantities were found by applying the correspondence principle to eqs 3-1 and 3-2

$$\bar{\sigma}_\theta = \frac{2\bar{p}b^2}{a^2-b^2}\left[\frac{\mathcal{Q}'\mathcal{Z}''-\mathcal{Z}'\mathcal{Q}''}{2\mathcal{Q}'\mathcal{Z}''+\mathcal{Z}'\mathcal{Q}''}\right] \qquad (3\text{-}3)$$

$$\bar{u}_r = \frac{\bar{p}b^2}{a^2-b^2}\frac{\mathcal{Q}'}{\mathcal{Z}'}\left[\frac{3\mathcal{Z}'\mathcal{Q}''}{2\mathcal{Q}'\mathcal{Z}''+\mathcal{Z}'\mathcal{Q}''}r+\frac{a^2}{r}\right] \qquad (3\text{-}4)$$

These relations were next applied to specific materials. It was postulated that the volume change was purely elastic, while the distortion behaved like a three-parameter solid.

Figure (3.3)

This assumption led to the following polynomial operators:

$$\mathcal{Q}''=1,\ \mathcal{Z}''=3K,\ \mathcal{Q}'=1+p_1 s,\ \mathcal{Z}'=q_0+q_1 s \qquad (3\text{-}5)$$

which were substituted into eqs 3-3 and 3-4.

After some lengthy arithmetic and transform inversions the following expressions were found:

$$u_r = \frac{pb^2}{a^2-b^2}\left\{\frac{3r}{6K+q_0}\left[1-e^{-\alpha t}\right] + \frac{3r\rho}{6K\rho_1+q_1}\, e^{-\alpha t} + \frac{a^2}{q_0 r}\left[1-e^{-\beta t}\right] + \frac{\rho a^2}{q_1 r}\, e^{-\beta t}\right\} \qquad (3\text{-}6)$$

and

$$\sigma_z = \frac{2pb^2}{a^2-b^2}\left\{\frac{3K-q_0}{6K+q_0}\left[1-e^{-\alpha t}\right] + \frac{3K\rho-q_1}{6K\rho+q_1}\, e^{-\alpha t}\right\} \qquad (3\text{-}7)$$

where

$$\alpha = \frac{6K+q_0}{6K+q_1} \quad ; \quad \beta = q_0/q_1 \qquad (3\text{-}8)$$

Appendix B contains a full derivation of these equations.

3.2.2 Finite Element Solution

In order to apply the finite element method, a slice was taken from the cylinder and discretized as shown in Fig (3.4). The material constants were found using the method detailed in section 2.2.2 and the problem was solved. The finite element solution was obtained using an initial timestep of 0.01 seconds which increased to a value of 0.1 seconds at the conclusion of the problem. Figs (3.5) through (3.9) present a comparison of the finite element results with the exact solutions. In each instance the variations from the exact were virtually nil. The worst-case variation was less than 1%

3.3 Summary

Based on the good fits obtained for both of the test problems, it was concluded that the finite element program was indeed valid, and could be applied to the intervertebral joint.

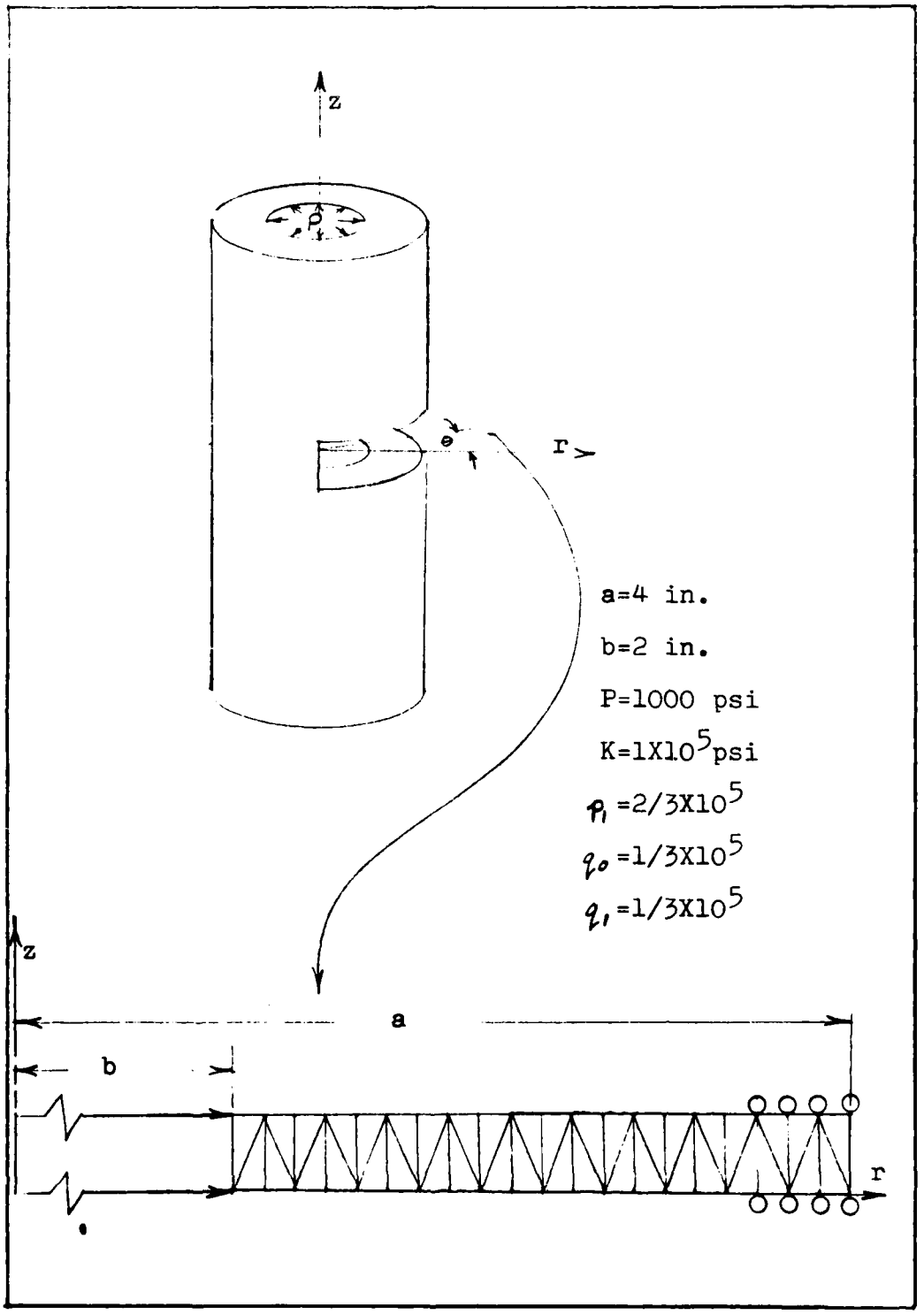

Figure 3.4 Thick-walled Cylinder

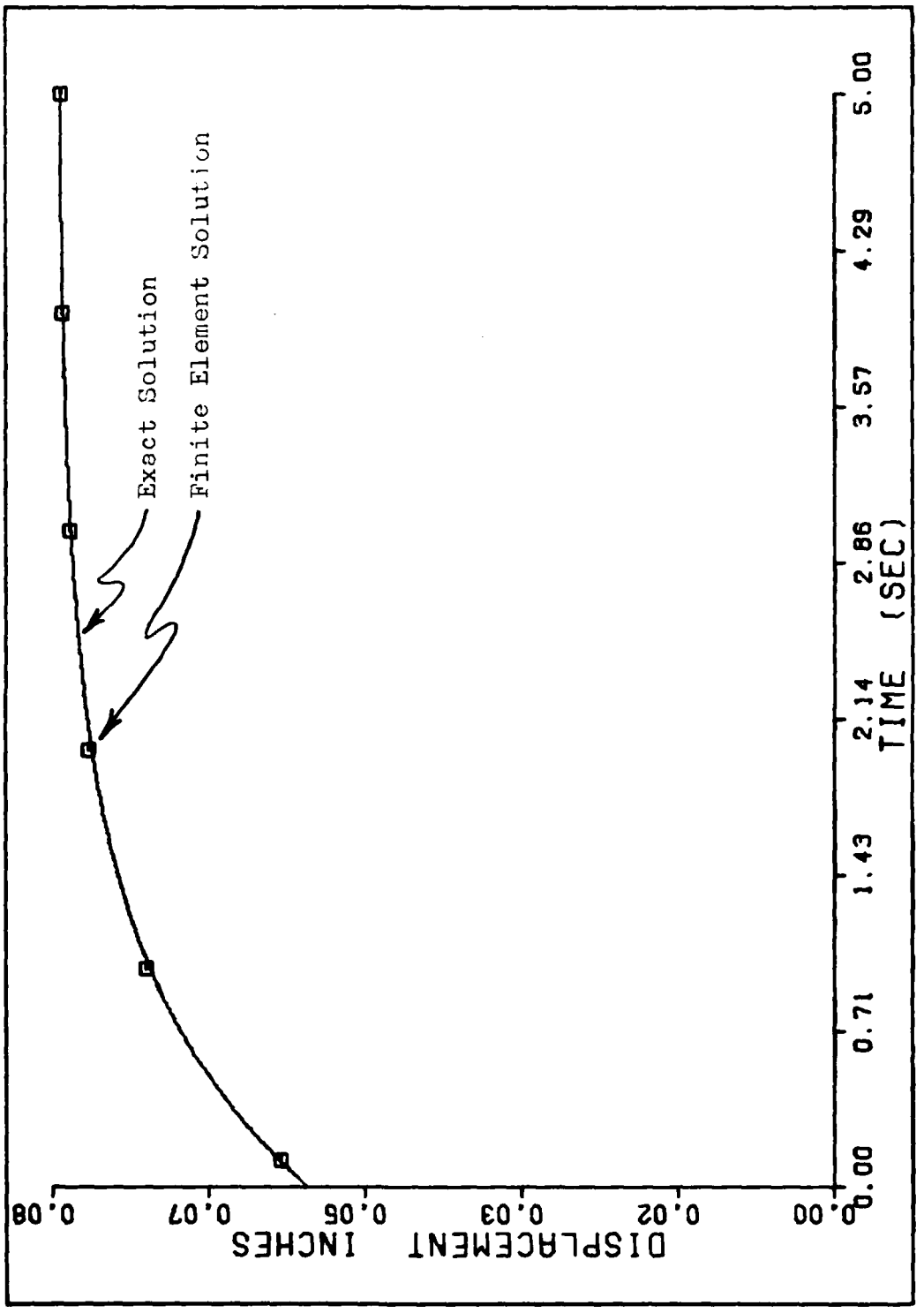

Figure 3.5 Thick-walled Cylinder u vs t r=2 in

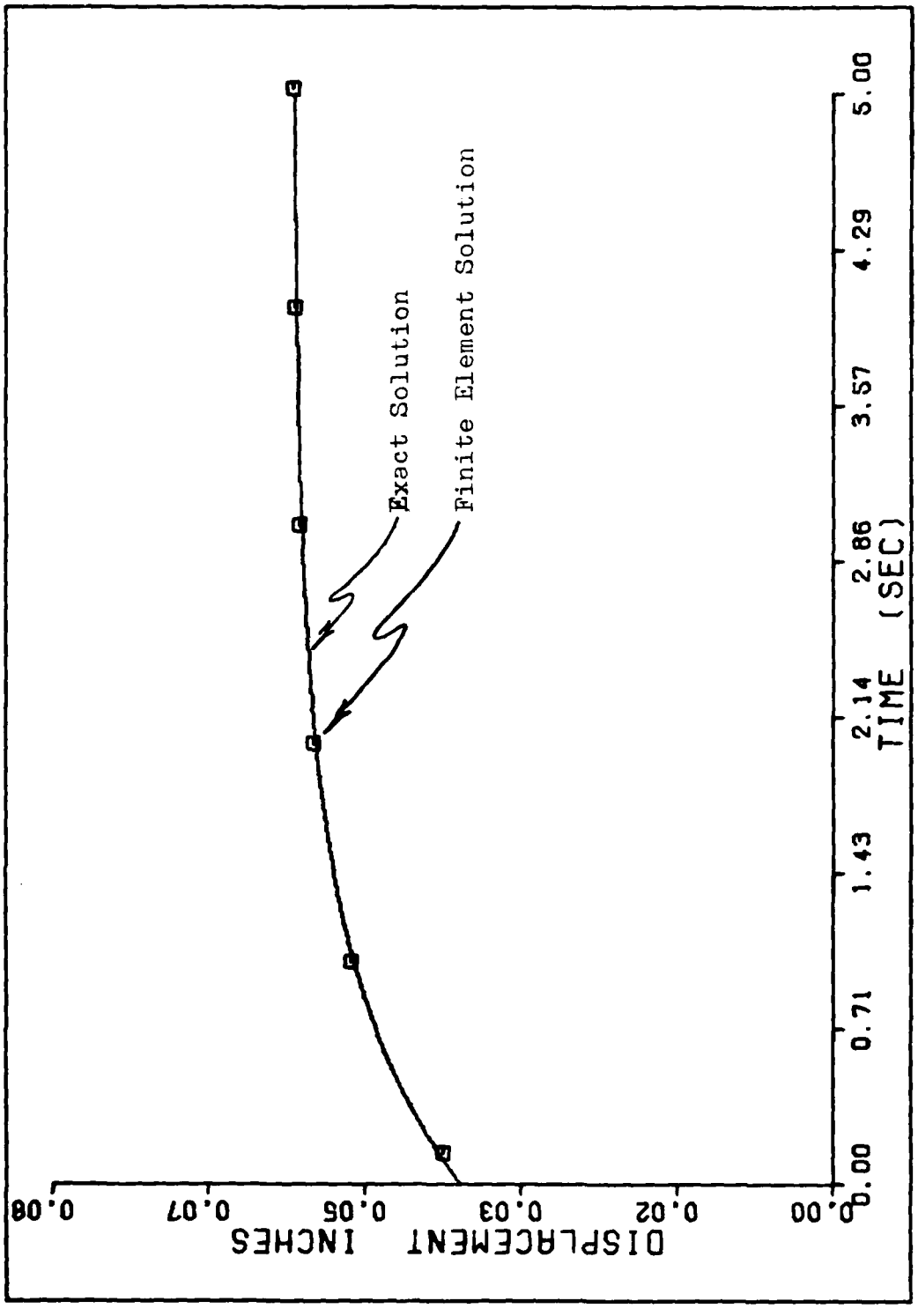

Figure 3.6 Thick-walled Cylinder u vs t r=3 in

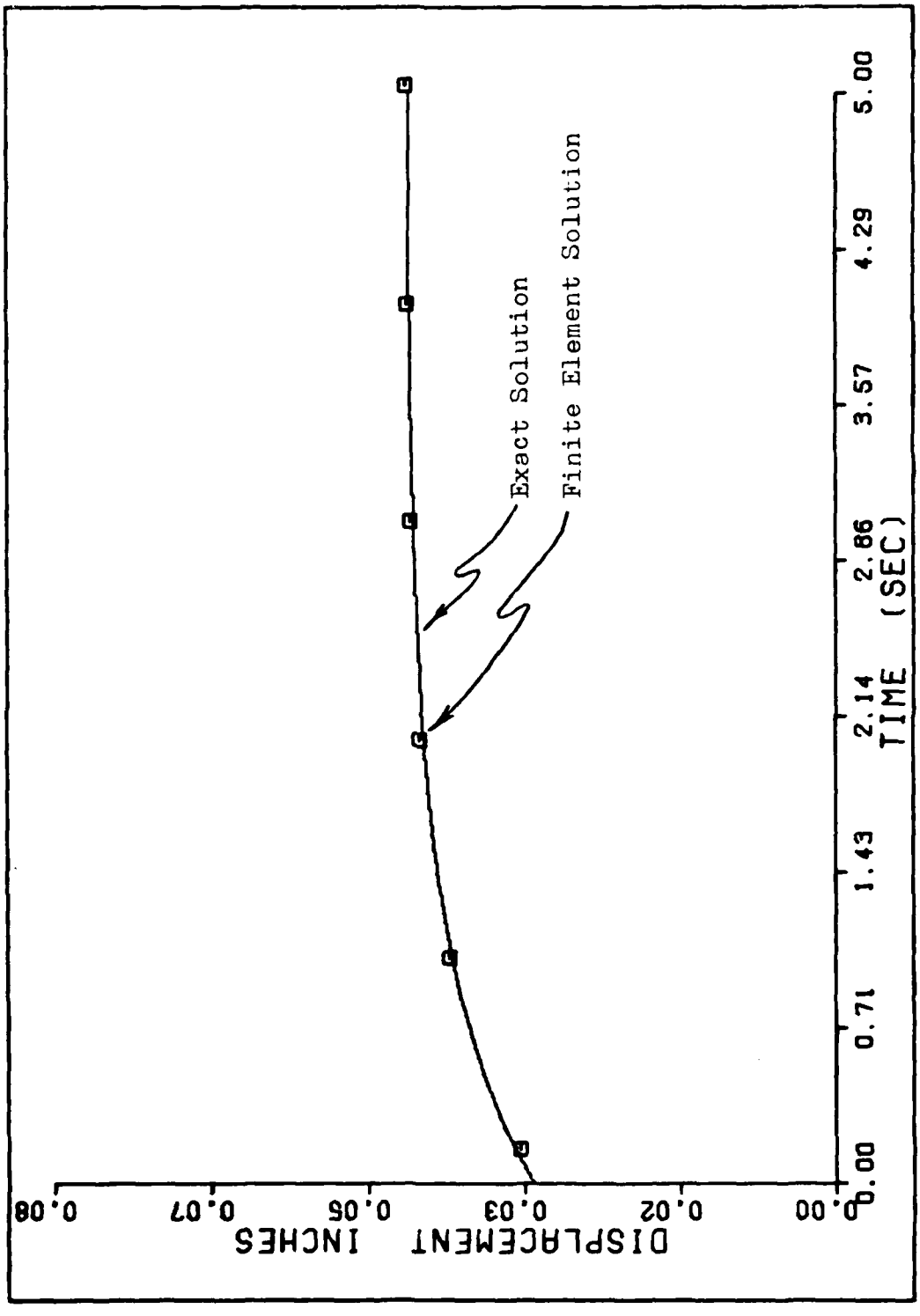

Figure 3.7 Thick-walled Cylinder u vs t r=4 in

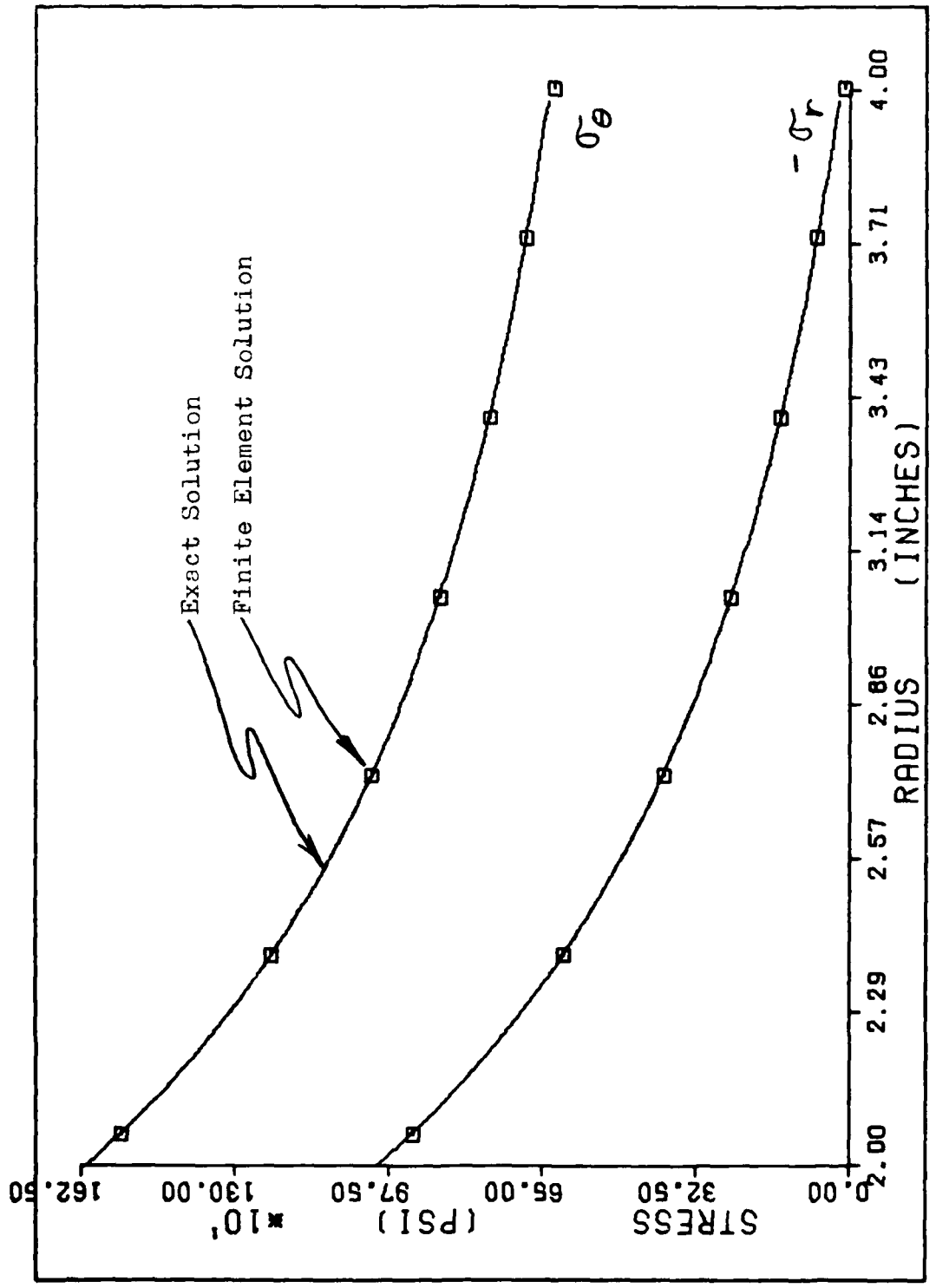

Figure 3.8 Thick-walled Cylinder σ_θ and $-\sigma_r$ vs r

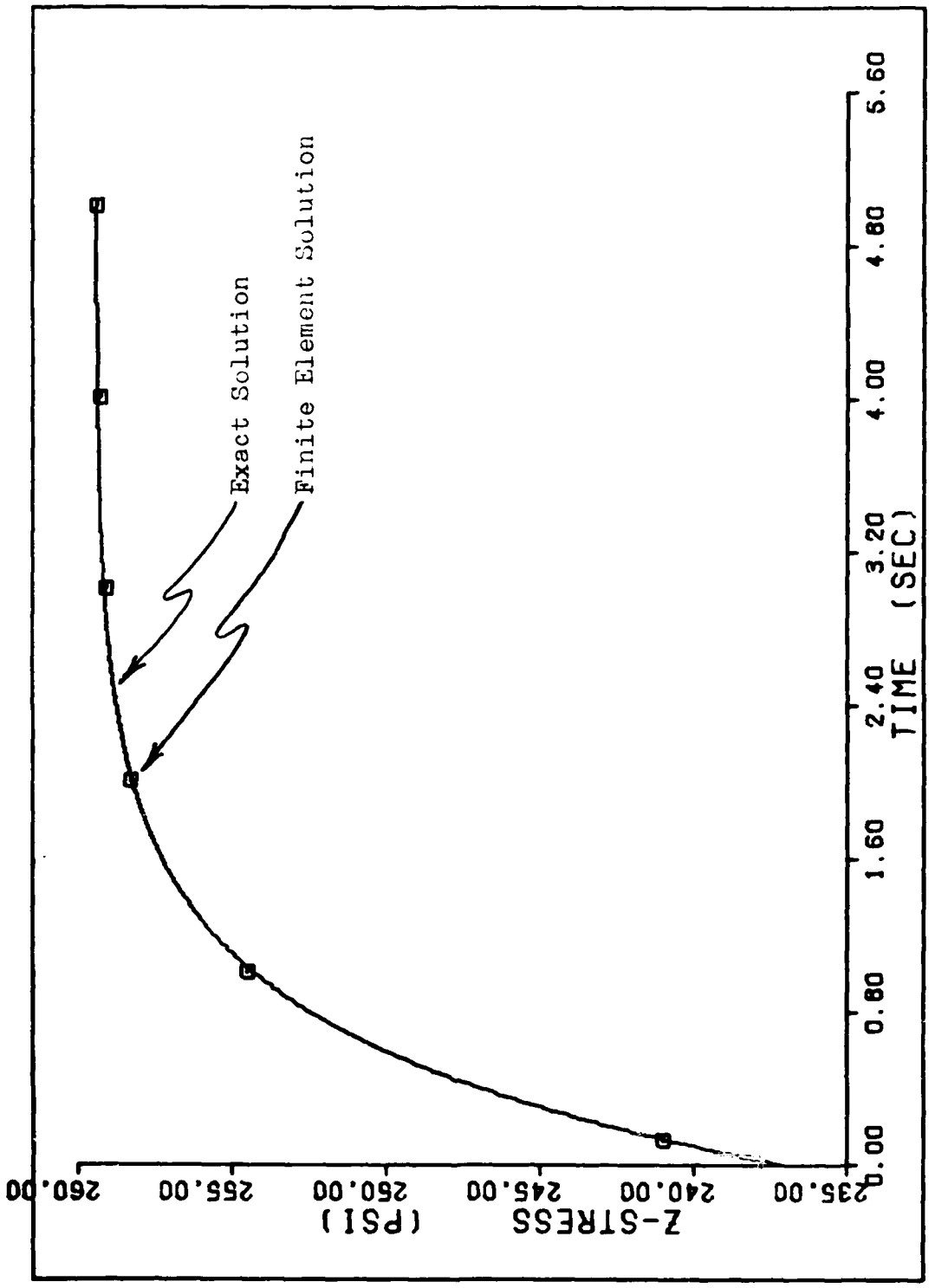

Figure 3.9 Thick-walled Cylinder σ_z vs t

CHAPTER 4

APPLICATION TO THE INTERVERTEBRAL JOINT

In the experiments performed by Kazarian et.al. (16), several intervertebral joint specimens were studied. These specimens were made by cutting the vertebral bodies parallel to the lines of demarcation between the discs and the bony end-plates at levels of maximum vertebral waisting. The specimens were then measured and placed in the test apparatus. Each was subjected to a dead weight load of 18.0 Kp (Kiloponds) for a period of time and the deflection of the top edge was recorded.

For the purpose of this finite element study, specimen number 65 (a T10-T11 segment) was used. So that comparisons with the experimental data could be made, the same 18.0 Kp load was applied to the finite element model as was applied to the test specimen.

4.1 Mesh Size and Material Constant Determination

In order to apply the finite element method to the intervertebral joint, it had to be discretized in such a way as to maximize the accuracy of the solution while minimizing the computer resources expended. To accomplish this, it was necessary to systematically reduce the mesh sizes until the stresses within the joint were observed to vary smoothly from one region to another. Additionally, since a major interest of this study was to observe the bone-disc interface, the bony end-plate region was used as a focal point during the mesh size reduction process. When the stresses within the bony end-plate were observed to vary by 15% from those of the previous mesh size, the model was considered to be refined enough to capture the trends of stress redistribution with time. Figure 4.1 shows the initial mesh used in the study.

Material properties for the trabecular and cortical bone were taken to be: E= 750Kp/Sqcm ν = 0.25 and E= 161000Kp/Sqcm ν= 0.25, respectively (4). Assignment of the viscoelastic material constants to the disc was done based on the properties derived in Ref. (16) i.e. E= 167.2Kp/Sqcm, q_0 = 64.6Kp/Sqcm, and q_1 = 1106000Kp-Sec/Sqcm. (See Fig 4.2 Ref. (16) fit to the experimental data) A problem in assigning these constants was immediately encountered due to the assumptions made in their derivation. Those assumptions being that the joint was a homogeneous one-dimensional rod.

Since the objective of this thesis was to represent the joint as a nonhomogeneous, axisymmetric structure, it was necessary to deviate from these constants.

The problem of inhomogeneity was approached first. If one has two elastic rods loaded as shown in Fig. 4.3, the first being made of a single material, while the other made of two materials, it is readily shown that the displacement

$$u(l) = \frac{Pl}{AE} \tag{4-1}$$

for the homogeneous rod and

$$u(l) = \frac{P(l-a)}{AE_2} + \frac{Pa}{AE_1} \tag{4-2}$$

for the nonhomogeneous rod. The value of E as given in ref. (16) was derived, in effect, by loading the specimen, observing the instantaneous displacement $u(l)$, and then applying eqn 4-1.

$$E = \frac{Pl}{Au(l)} \tag{4-3}$$

This approach was extended to the nonhomogeneous rod by equating the right-hand sides of eqs 4-1 and 4-2.

$$\frac{Pl}{AE} = \frac{P(l-a)}{AE_2} + \frac{Pa}{AE_1} \tag{4-4}$$

Here, all the values were known with the exception of E_1, which was found by simple algebra to be

$$E_1 = \frac{a E E_2}{l(E_2 - E) + aE} \qquad (4\text{-}5)$$

Since the vertebral body was assumed to be linearly elastic, the constants q_0 and q_1 for the disc were simply proportioned by a/l to obtain

$$q_0 = 23.34 \text{ Kp/Sqcm}$$

$$q_1 = 400{,}000 \text{ Kp-Sec/Sqcm}$$

Poisson's ratio for the disc was taken to be 0.48 (4).

These material constants were assigned, and a computer run was made. The instantaneous displacement of the top edge of the joint at the line of rotational symmetry was observed to be 0.003 cm, which varied significantly from the experimental value of 0.014 cm. Furthermore, as time proceeded, the displacement remained nearly constant. At the end of 167 minutes simulation time, a value of only 0.004 cm was reached, while the experimental deflection was 0.023 cm at that time. These large variations from the experimentally observed data were concluded to be a consequence of having determined E, q_0, and q_1 for the disc based on the assumption that the joint was a one-dimensional rod.

Before the mesh size reduction could proceed, the values of E, q_0, and q_1 had to be found which would more closely match the experimental results. It was noted that the instantaneous displacement was dependant on the value of E but independant of q_0 and q_1. The first step, therefore, was to vary the E value until the model matched

the experimental displacement at t=0. This was done quite readily using a trial and error method. The value of E which best represented the instantaneous deflection, was found to be 7.5 Kp/Sqcm. Fig 4.4 shows the displacement vs time plot based on this E value.

The values of q_0 and q_1 were found by a similar method. It was noted that the q_1 value controlled the slope of the displacement vs time curve, while the q_0 value had more influence on the displacement limit approached as time increased. Fig 4.5 and 4.6 show some intermediate results obtained by varying q_0 and q_1. The values for q_0 and q_1 which best represented the data were found to be q_0 =0.015 Kp/Sqcm and q_1 =28,150 Kp-Sec/Sqcm.

With these material constants, the mesh size reduction process was continued. Figures 4.7 and 4.8 show some intermediate mesh sizes. Whereas, at each reduction, the instantaneous deflections varied little from those obtained with the course mesh, those observed as time progressed began to deviate from the experimental data. These observations revealed that the value of E which was derived from the course mesh model was good, but the values of q_0 and q_1 needed more refinement. Therefore, as the mesh size was further reduced, minor adjustments to the q_0 and q_1 values were made. This process continued until the q_0 and q_1 values showed less model dependance, and the stresses within the joint varied smoothly from one region to another. Furthermore, the stresses in the bony end-plate were

observed to vary by less than 15% from those of the previous mesh size. Figure 4.9 presents the final mesh size, while Fig 4.10 shows the displacement vs time plot based on the final values of q_0 =.01 Kp/Sqcm and q_1 =27000 Kp-Sec/Sqcm.

4.2 Displacement Profiles

In order to visualize the displacements throughout the joint as time increases, plots of the deformed shape were made at convenient intervals. Figure 4.11a presents the undeformed shape, while Figs 4.11b,c,d show the shapes at time=0.0, 80.0, and 160.0 minutes respectively. In each of the figures, the deformations were magnified by a factor of 2 so that they could be more readily observed.

It was noted that because of the large disparity between the elastic moduli of the vertebral body and the disc, the greatest instantaneous deformation presented itself in the disc. As time progressed, this condition became even more pronounced in support of the assumption that all viscoelastic effects were contributed to the disc.

Note that the disc appears to be "squeezed" outwardly in the radial direction. As it moves outward in time, one would expect that there would be an accompanying increase in shear stress along the disc-bone interface. Additionally, since the disc is constrained from moving radially at the line of rotational symmetry, one would expect the radial component of direct stress to show an increase in tension as

the disc displaces outwardly. This outward movement also appears to cause a "twisting" of the vertebral body. That is, the wall of the cortical bone on the exterior of the body is being displaced outwardly at the disc-bone interface, while the top edge is displacing downward and inward. One would expect this "twisting" to cause the trabecular region to be placed in a state of compression that would increase with time.

In the following section, the actual stress redistributions are presented and appear for the most part to follow the stresses one would expect from intuitive arguments.

4.3 Stress Redistributions

The variation of shear stress through the joint was of interest in determining the final mesh size. Vertical profiles of shear were taken at two radii: r=0.625 cm and r=1.5 cm, and plotted to observe the variations. These profiles are presented for t=0.0 in Figures 4.12 and 4.13. It was noted that the bony end-plate served as a boundary in which the shear in the two relatively soft adjacent regions underwent a sign change.

In addition to these vertical profiles, horizontal profiles of all the stress components were taken at three different joint levels: within the disc, the bony end-plate, and the trabecular bone region just superior to the bony

end-plate. Figures 4.14 through 4.25 present these profiles for times varying from 0.0 to 160.0 minutes. From these stress profiles, a number of observations were made.

Figure 4.14 reveals that the radial component of stress in the disc increased with time and at a radius of 2.2 cm, the increase after 160.0 minutes was approximately 30%. This increase was also noted in the circumferential or hoop stress component (Fig 4.16). The axial stress component (Fig 4.15) was seen to increase by about 7% overall during the 160.0 minute interval. The shear stress (Fig 4.17) showed an interesting trend. For radial values from 0.0 to about 1.75 cm, the shear increased with time, while for greater radial values, it tended to decrease or relax. This trend to relax was *not* predicted by intuitive arguments, but is concluded to be a result of the disc-bone interface geometry. That is, because the interface is a curved surface rather than a flat one, intuition fails to accurately predict the stress redistribution.

In the bony end-plate, where the greatest interest of this study was centered, the first observation one makes is that in each case, the stress components are of a much larger magnitude than for any other joint region. This points to the fact that the disc-bone interface is an area which serves an important role in the overall integrity of the human intervertebral joint. Furthermore, as time progressed, the stresses underwent some significant changes, which reveal the region to be very active during creep. The

radial component (Fig 4.18) increased by about 8% overall during the simulation. In the shear stress component (Fig 4.21) there was an overall tendancy to increase in absolute value. This trend was most pronounced at r=2.0 cm where the increase was about 20%. The hoop stress (Fig 4.20) increased for radial values from 0.0 to 1.5 cm and relaxed for radial values greater than 1.5 cm. The stress reduction was most pronounced at a radius of 2.2 cm where a 9% change was observed. Figure 4.19, which depicts the axial stress component, shows the bony end-plate to be in a state of compression axially. This component showed a tendancy to relax with time, with the reduction on the order of 9% overall.

In the trabecular bone region, the stresses (Figs 4.22-4.25) remained virtually constant. It should be noted that the final data point on these plots near r=2.40 cm is in the region of the vertebral body which is composed of cortical bone. In that region (as was the case with the bony end-plate) the stresses did vary with time.

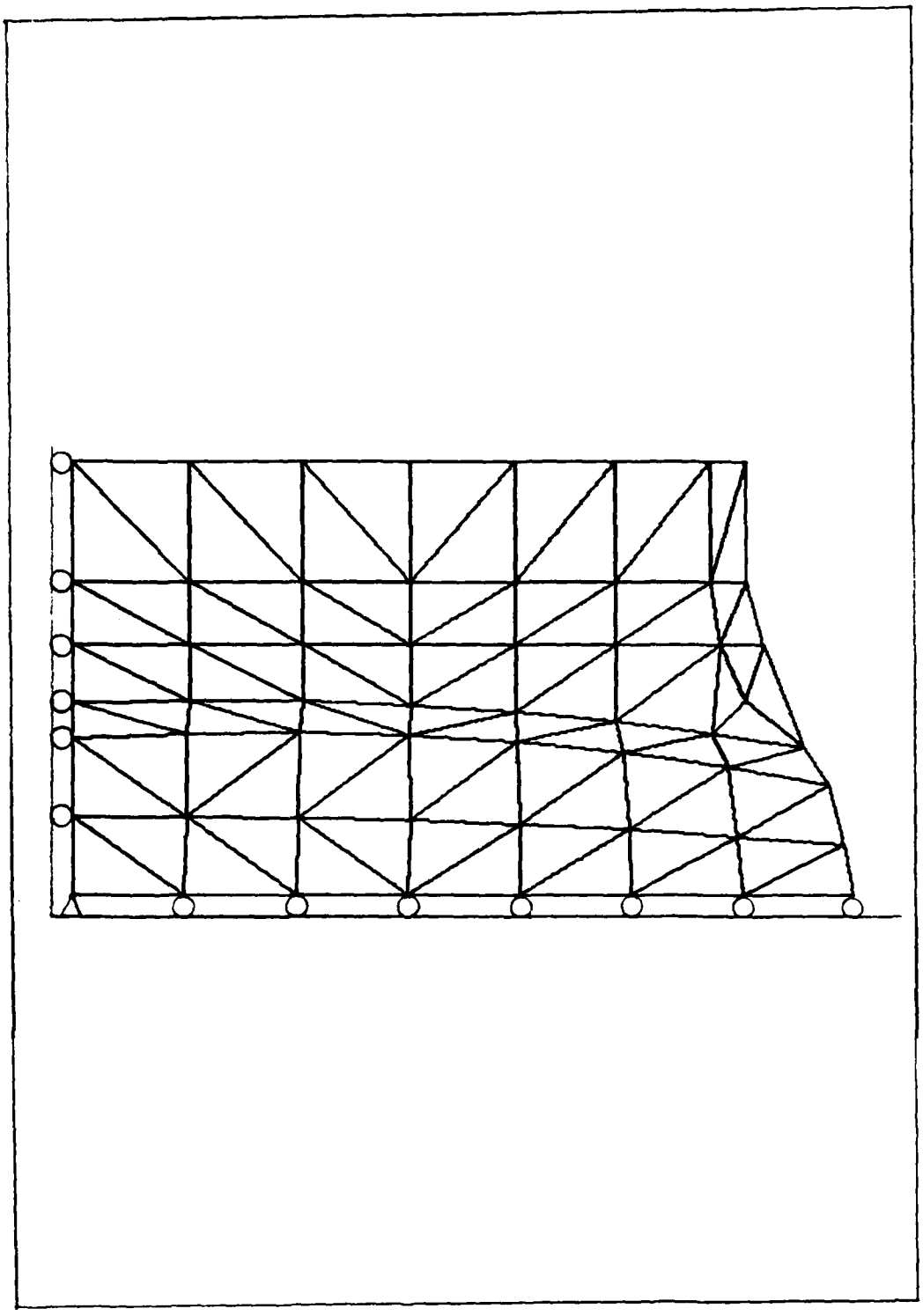

Figure 4.1 Initial Mesh Size

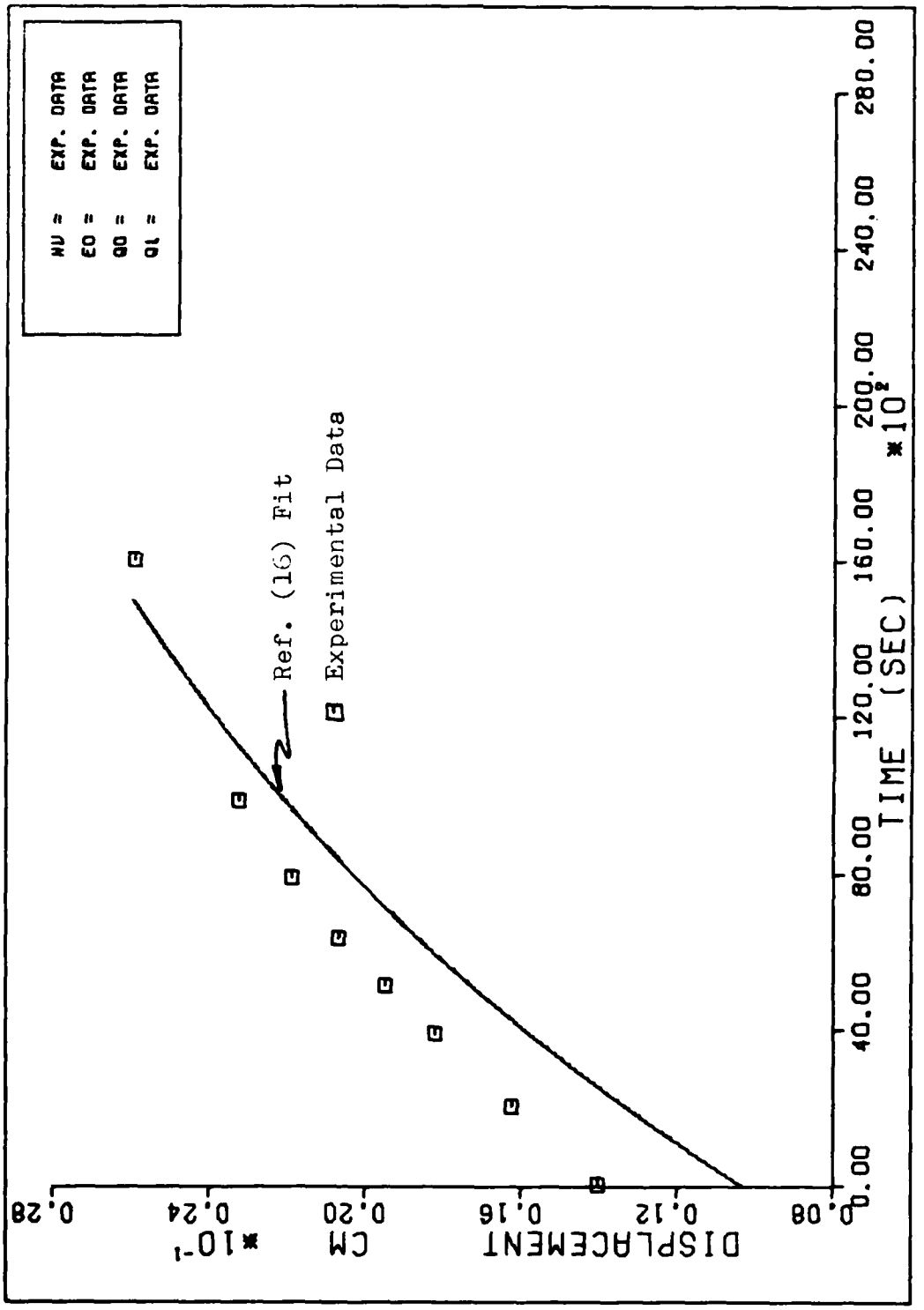

Figure 4.2 Ref. (16) Fit to the Experimental Data

a. Homogeneous Axial Rod

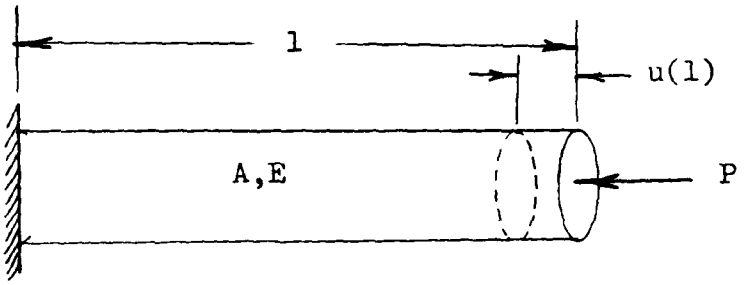

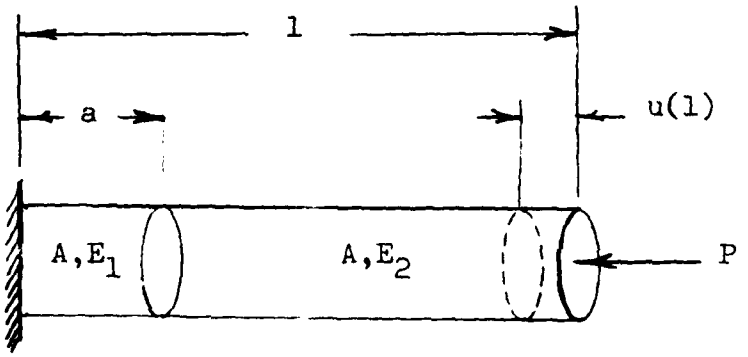

b. Non-homogeneous Axial Rod

Figure 4.3 Two Elastic Rods

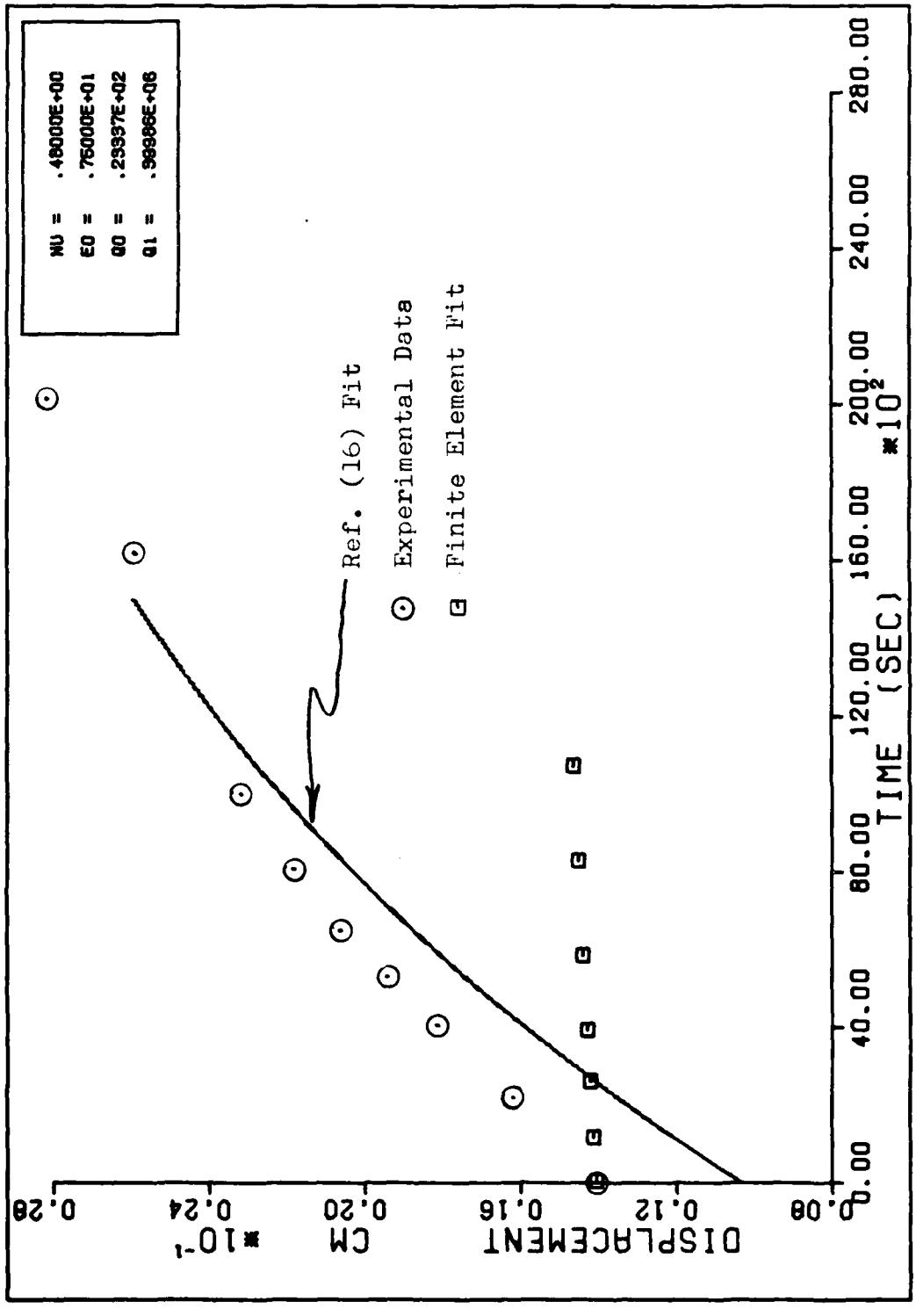

Figure 4.4 Displacement vs Time Intermediate Results

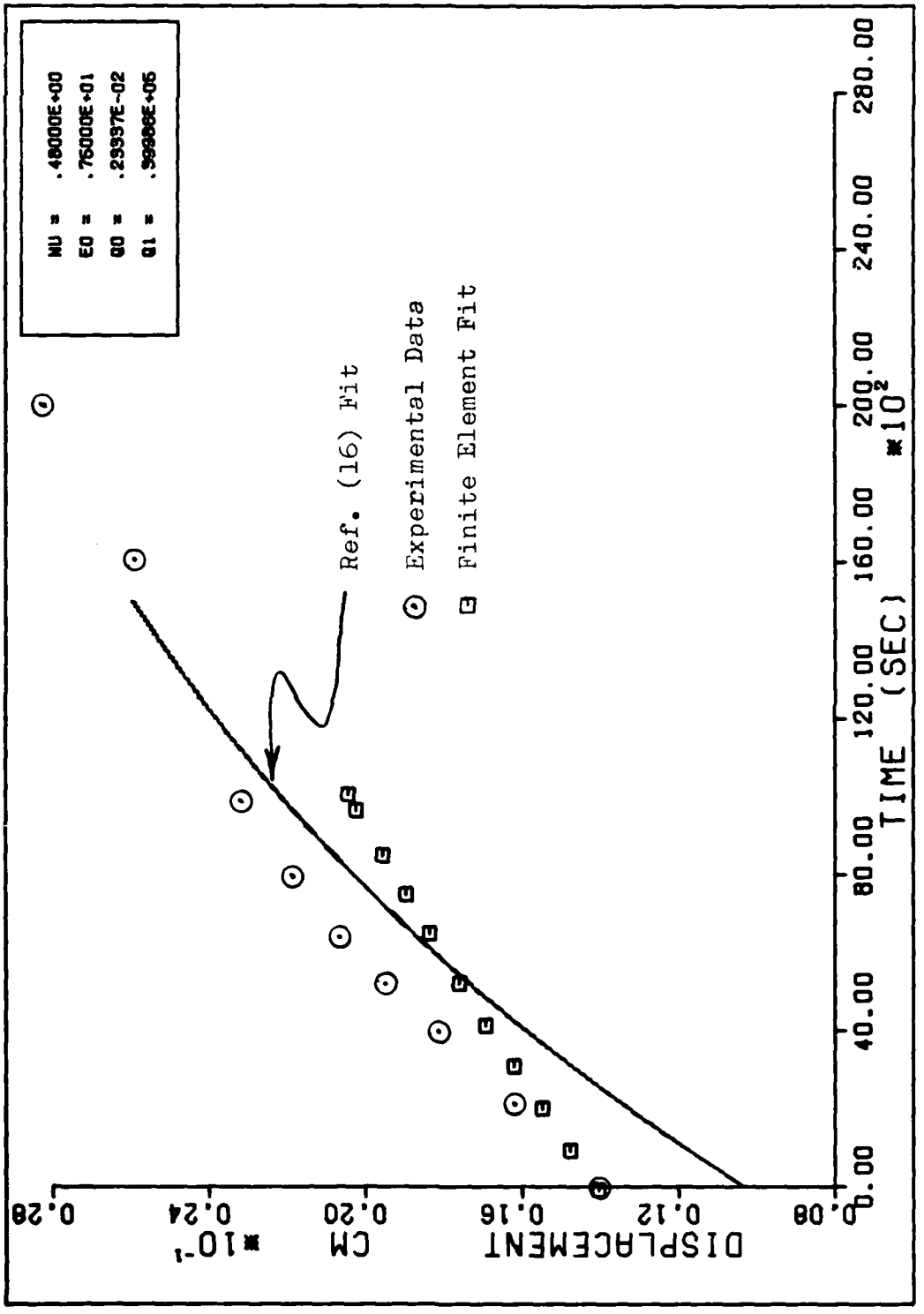

Figure 4.5 Displacement vs Time Intermediate Results

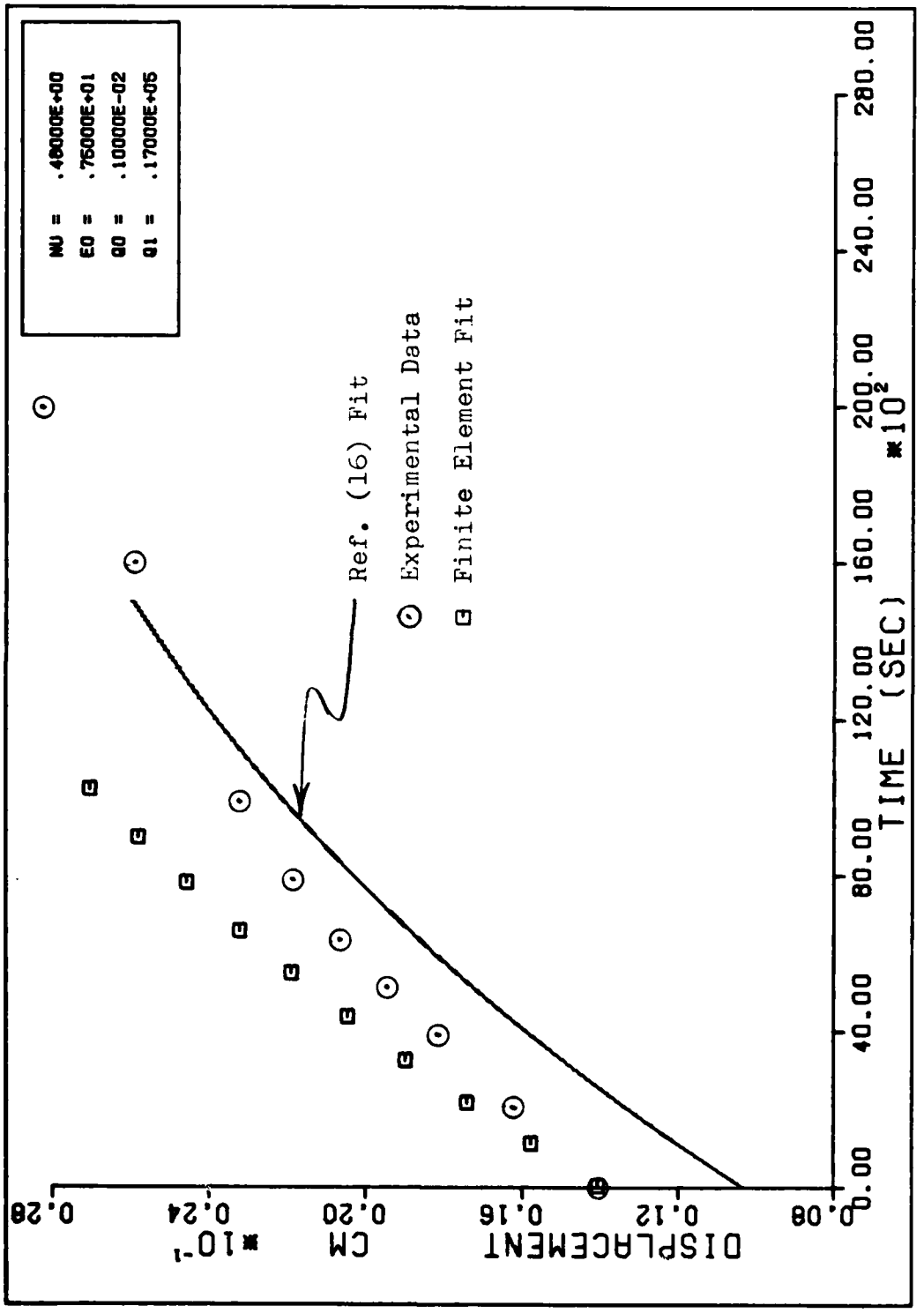

Figure 4.6 Displacement vs Time Intermediate Results

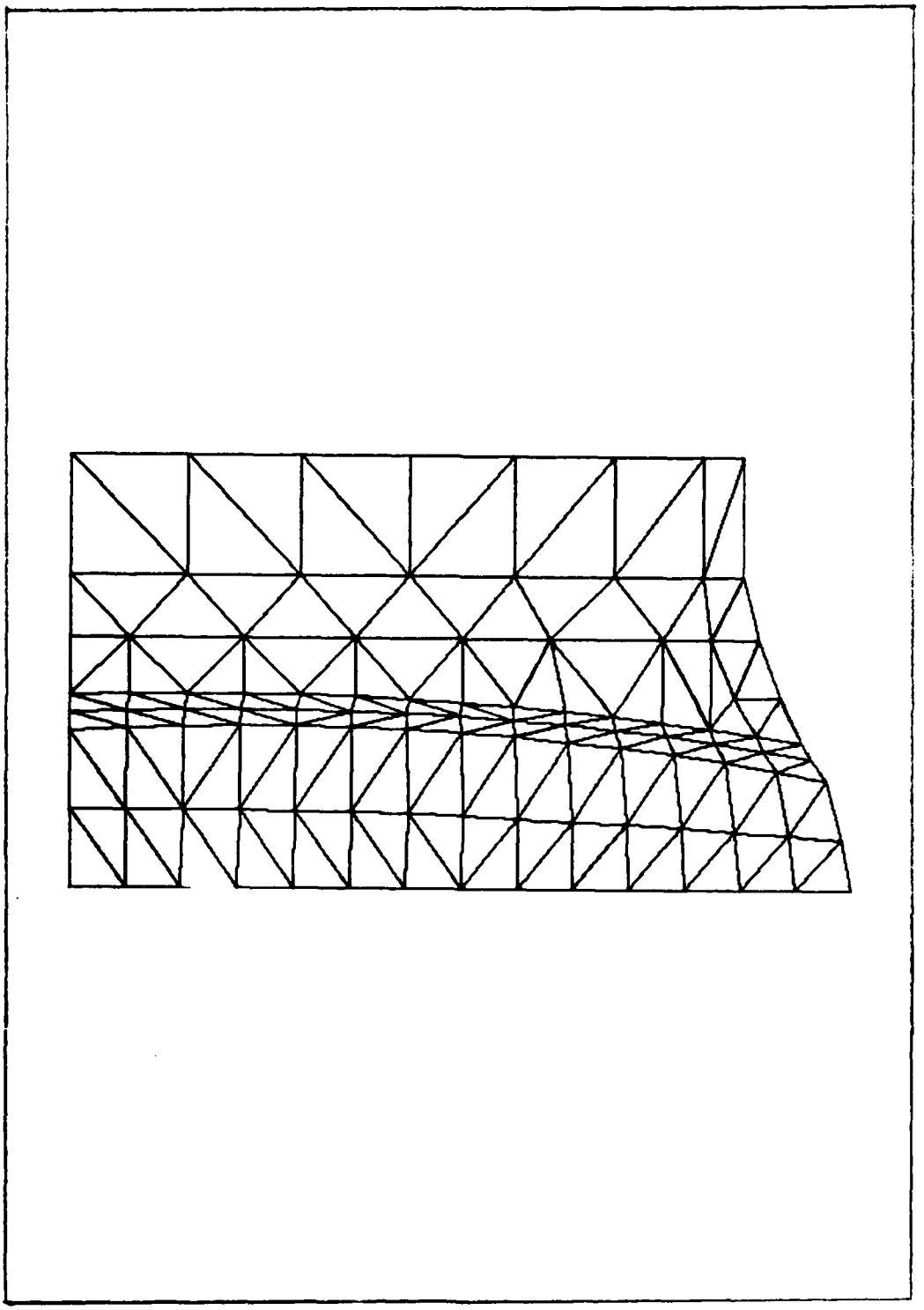

Figure 4.7 Intermediate Mesh Sizes

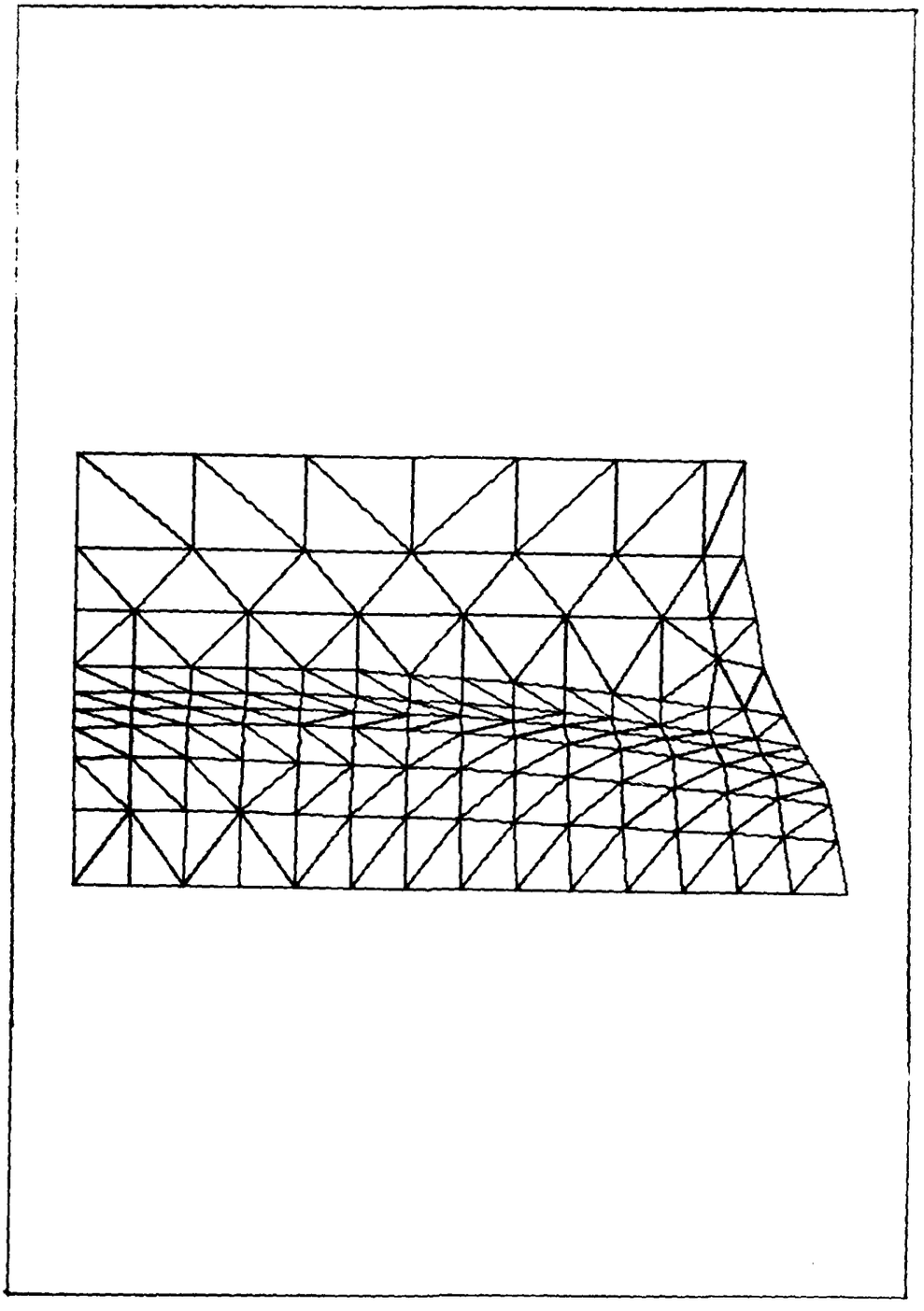

Figure 4.8 Intermediate Mesh Sizes

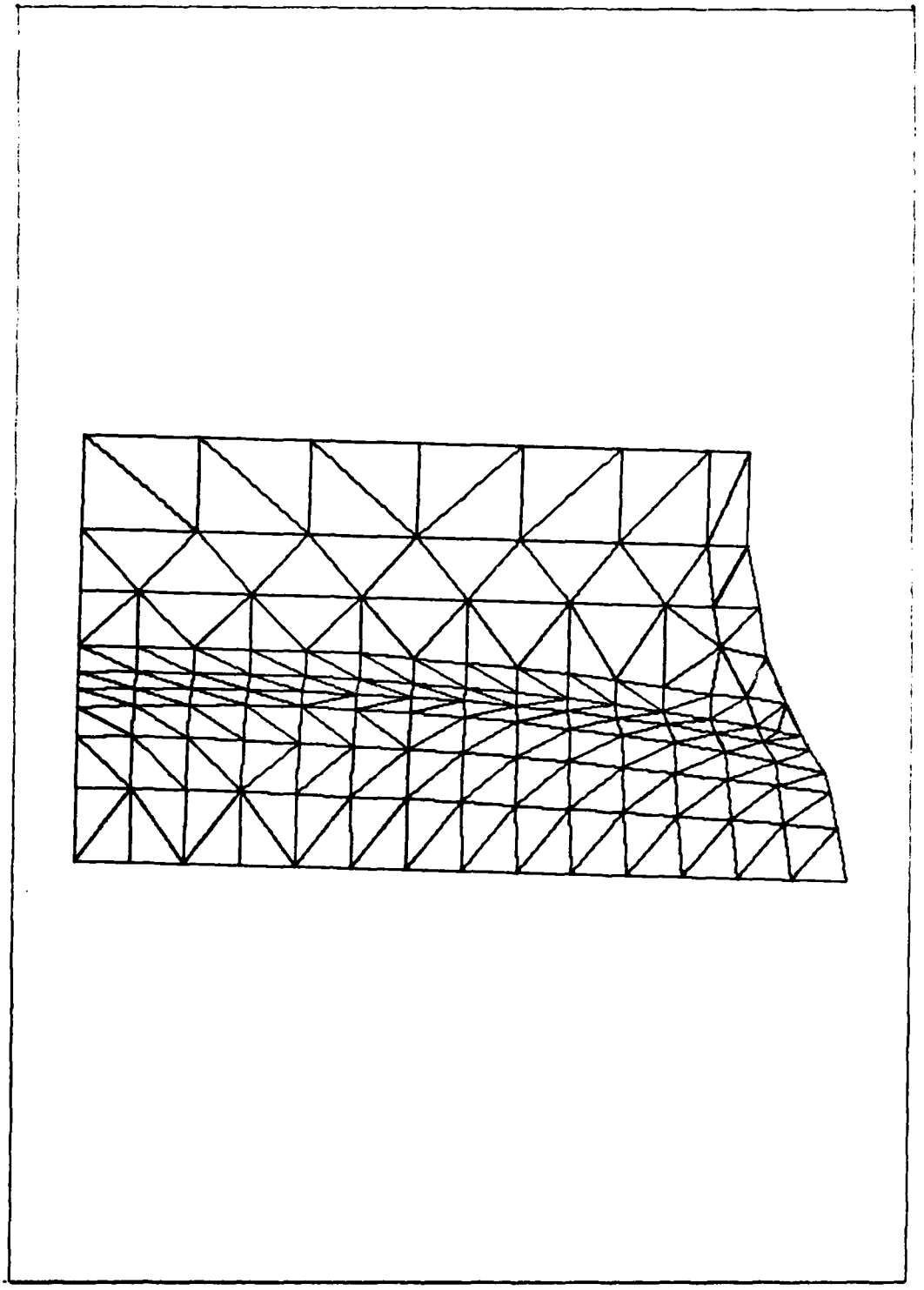

Figure 4.9 Final Mesh Size

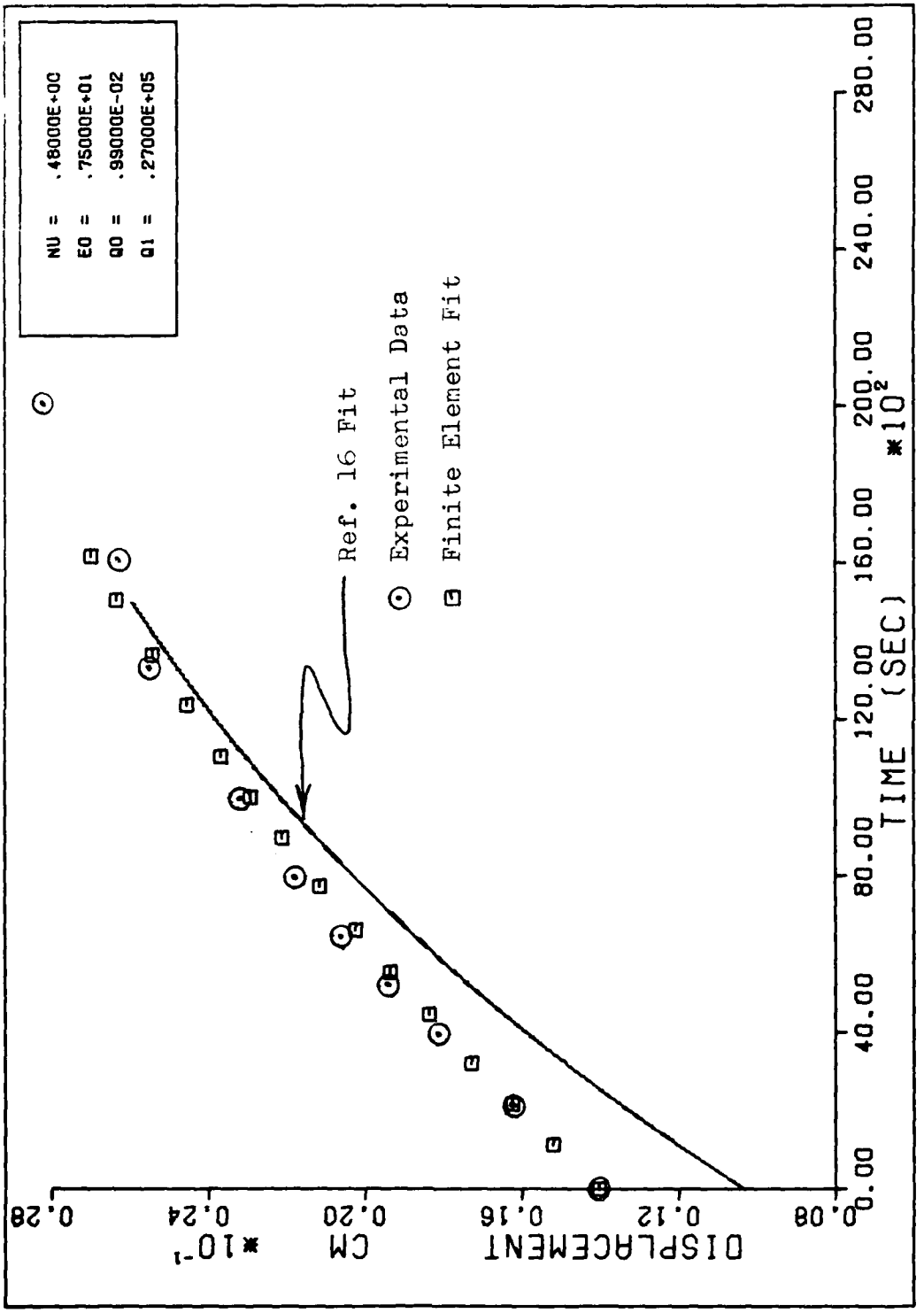

Figure 4.10 Displacement vs Time Final Results

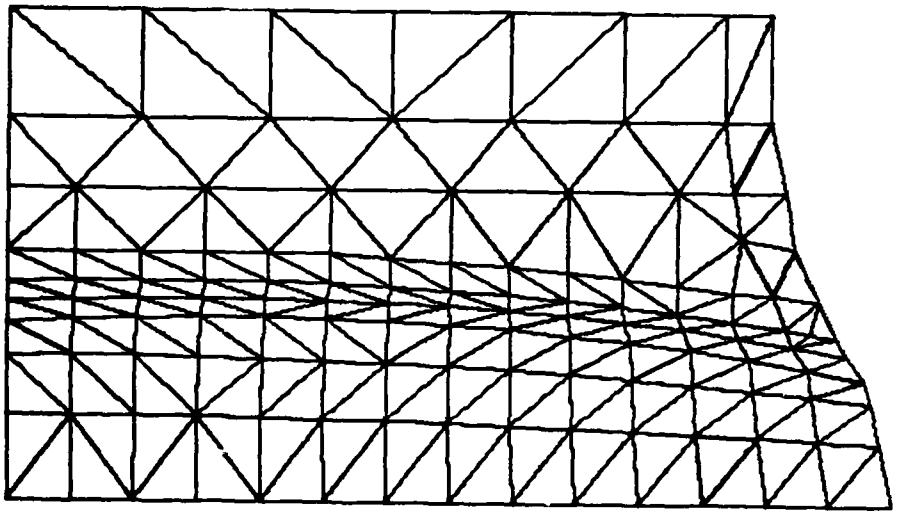

Figure 4.11a Undeformed Shape t=0-

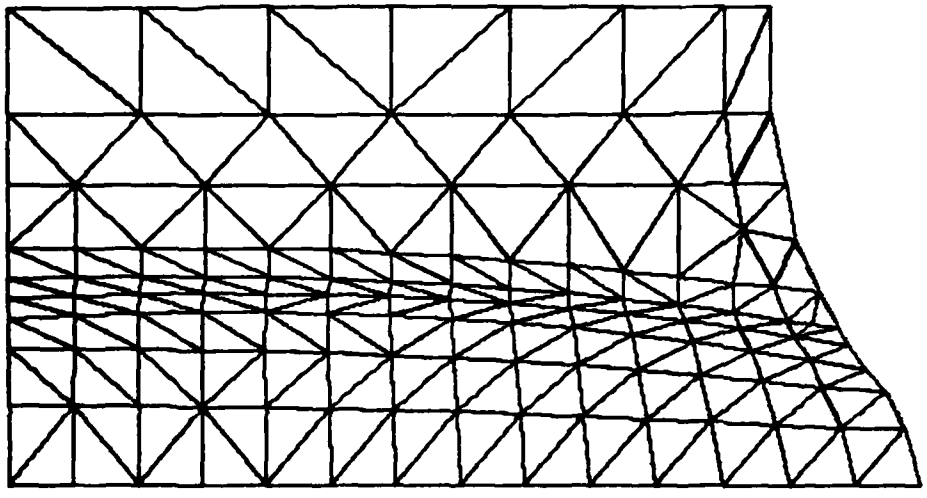

Figure 4.11b Deformed Shape t=0+

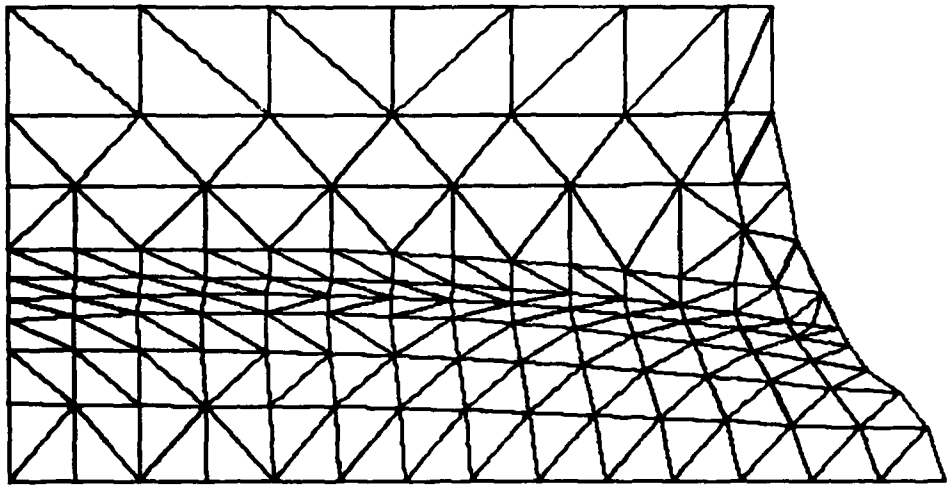

Figure 4.11c Deformed Shape t=80 min.

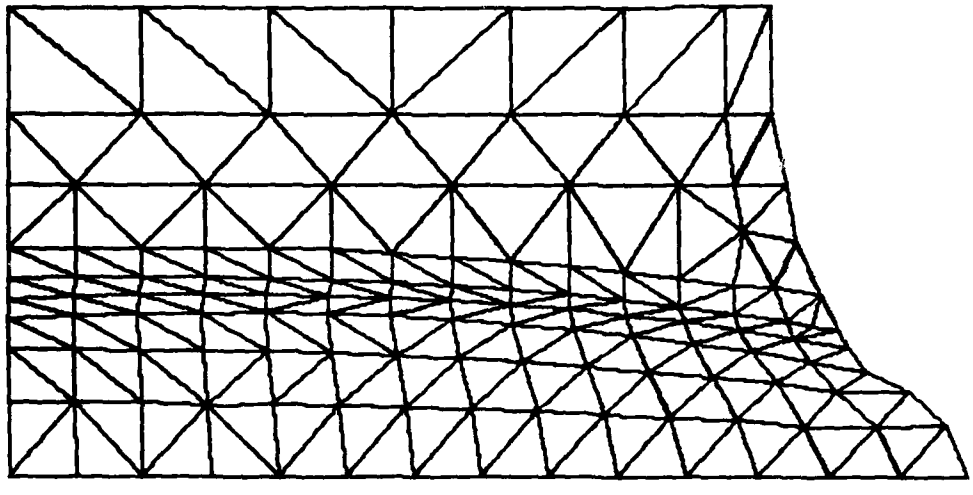

Figure 4.11d Deformed Shape t=160 min.

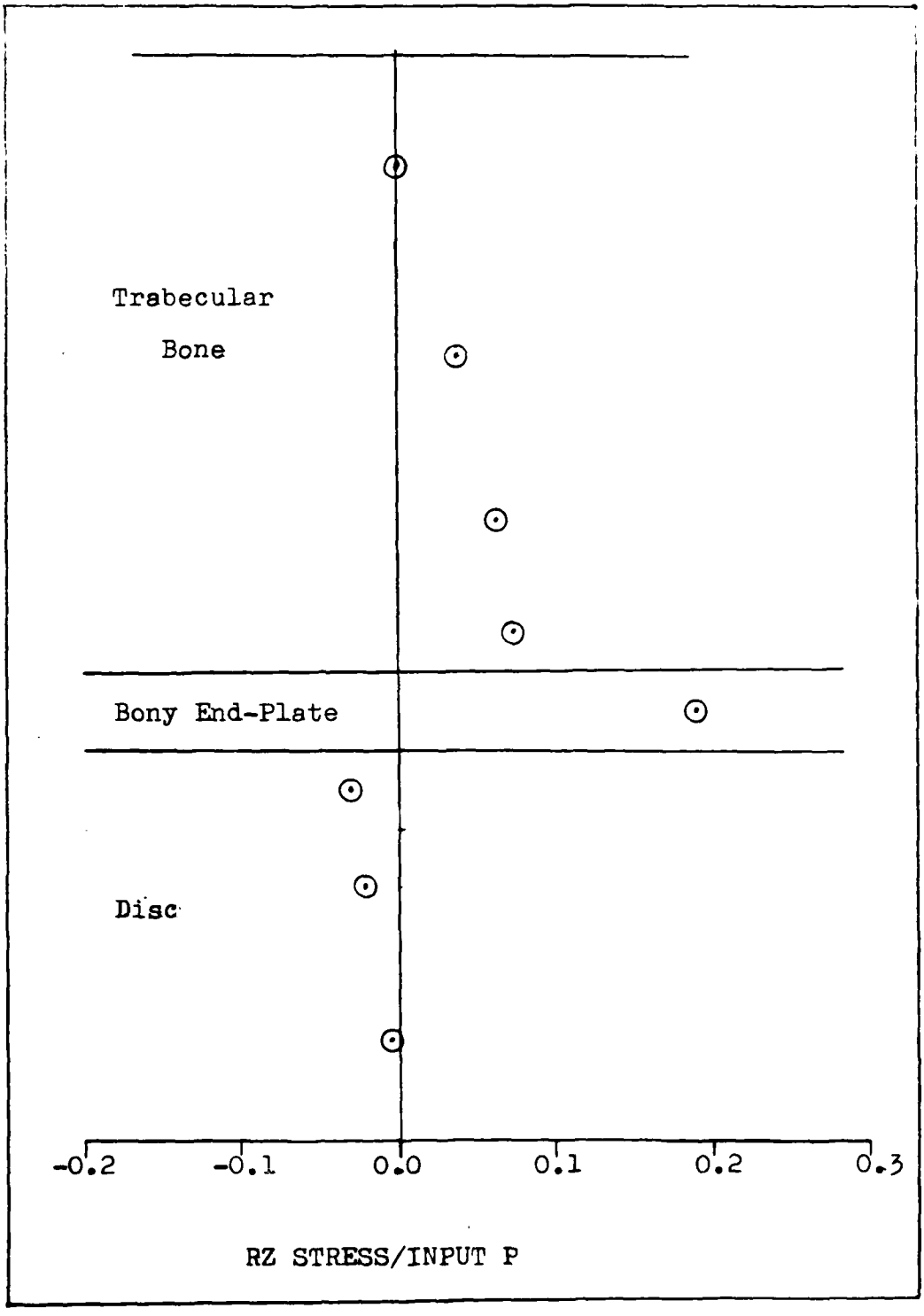

Figure 4.12 Shear Stress Profile r=0.625

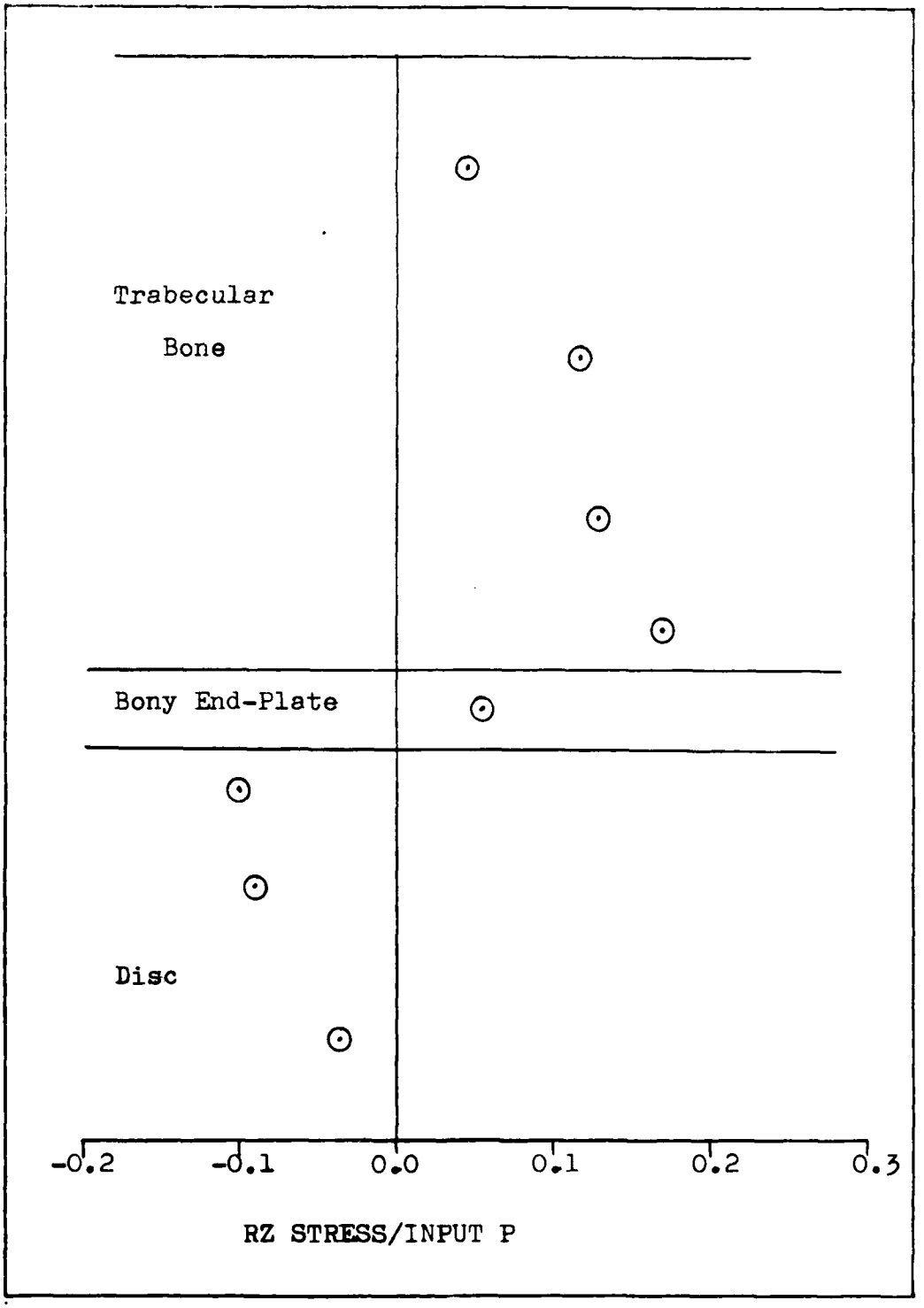

Figure 4.13 Shear Stress Profile r=1.52

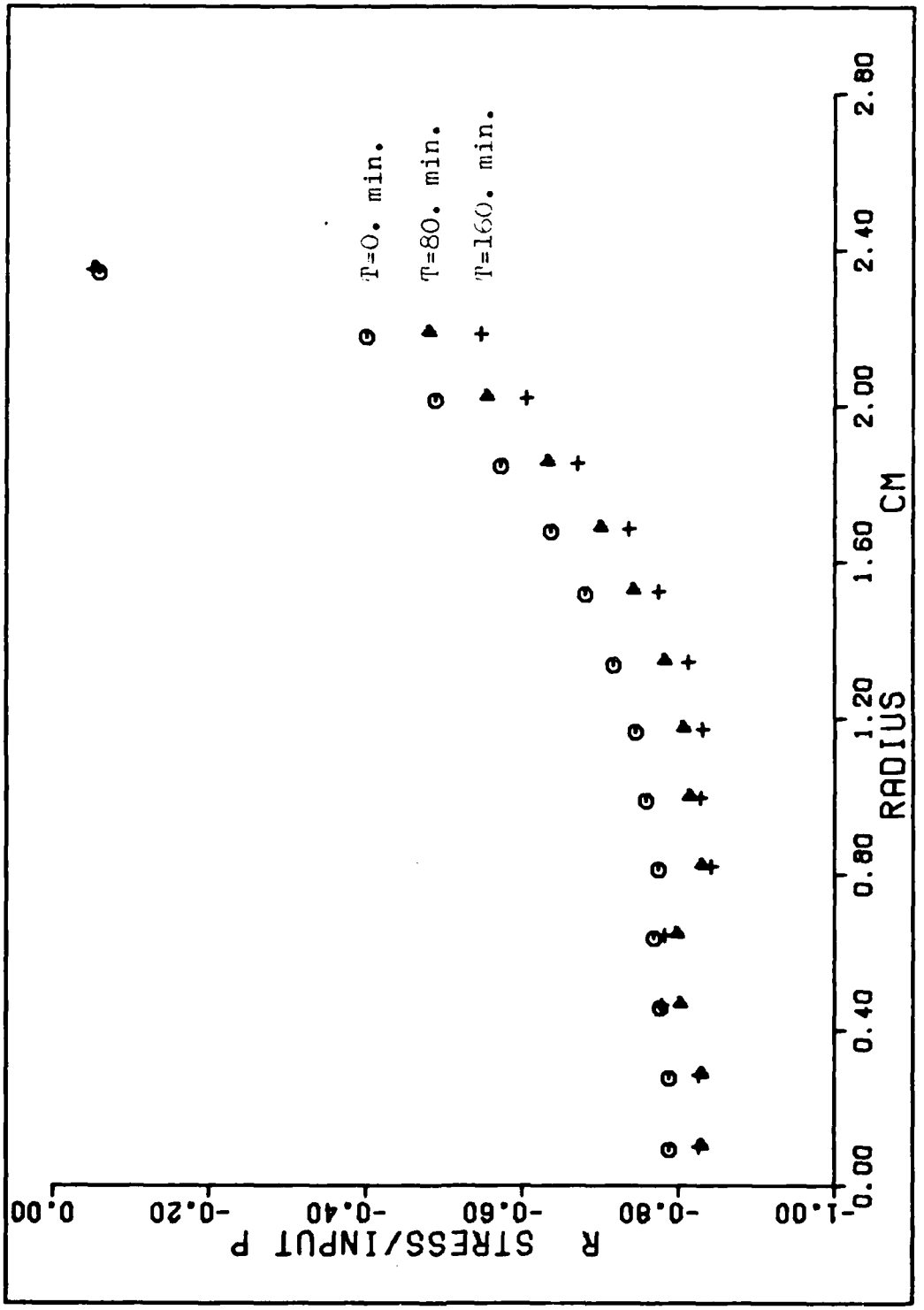

Figure 4.14 R Stress/Input P--Disc
(σ_r)

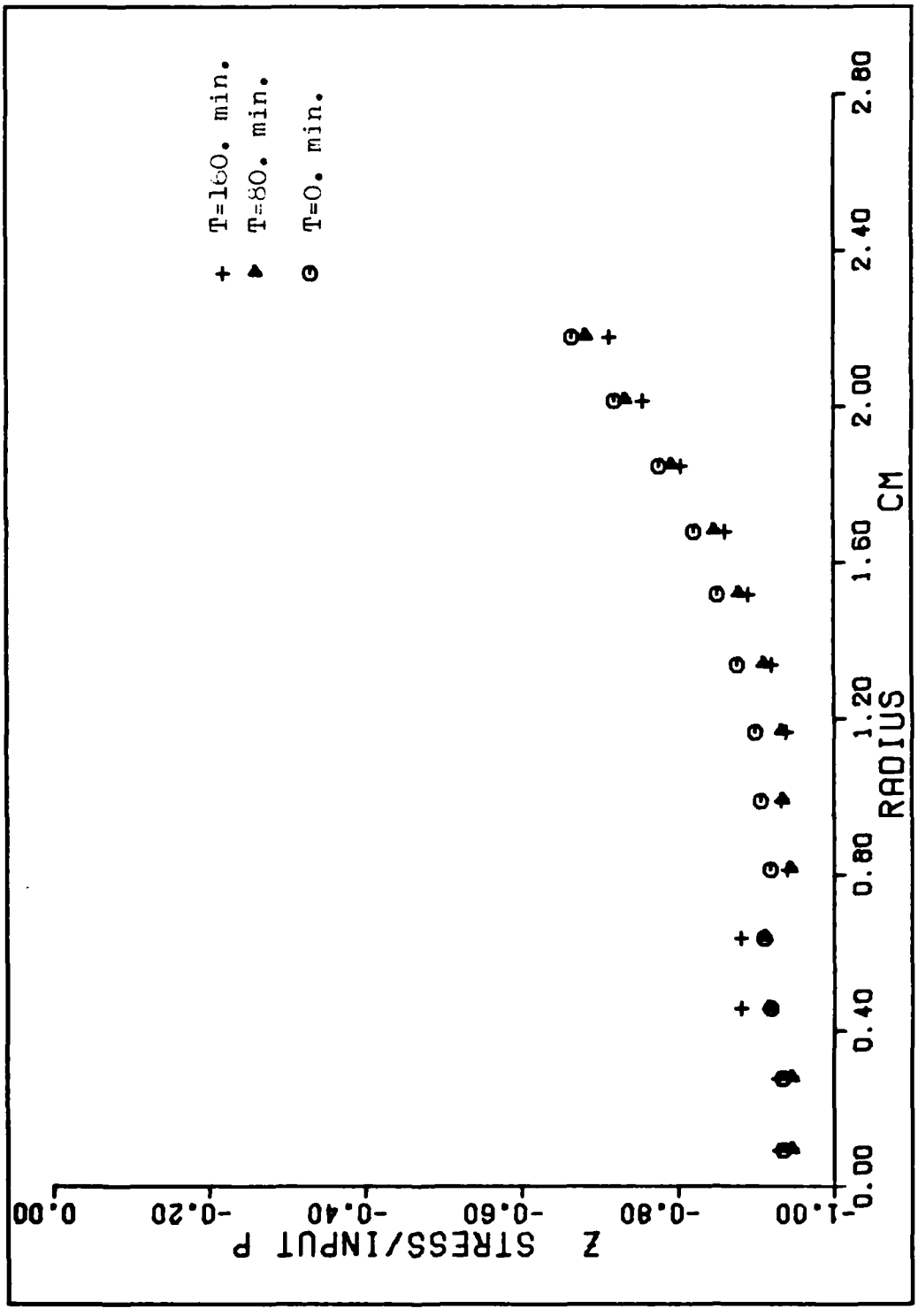

Figure 4.15 Z Stress/Input P--Disc

(σ_z)

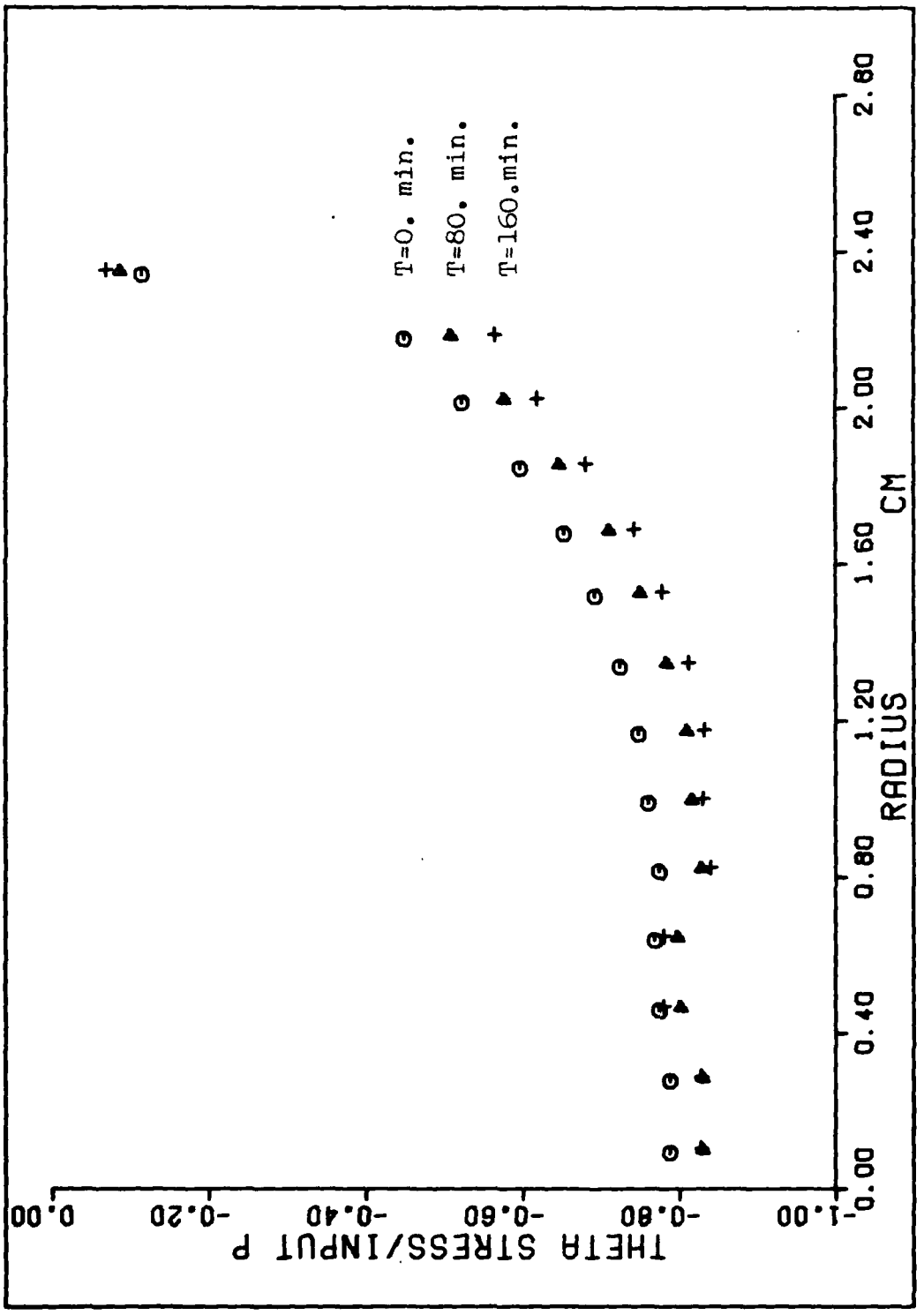

Figure 4.16 Theta Stress/Input P--disc

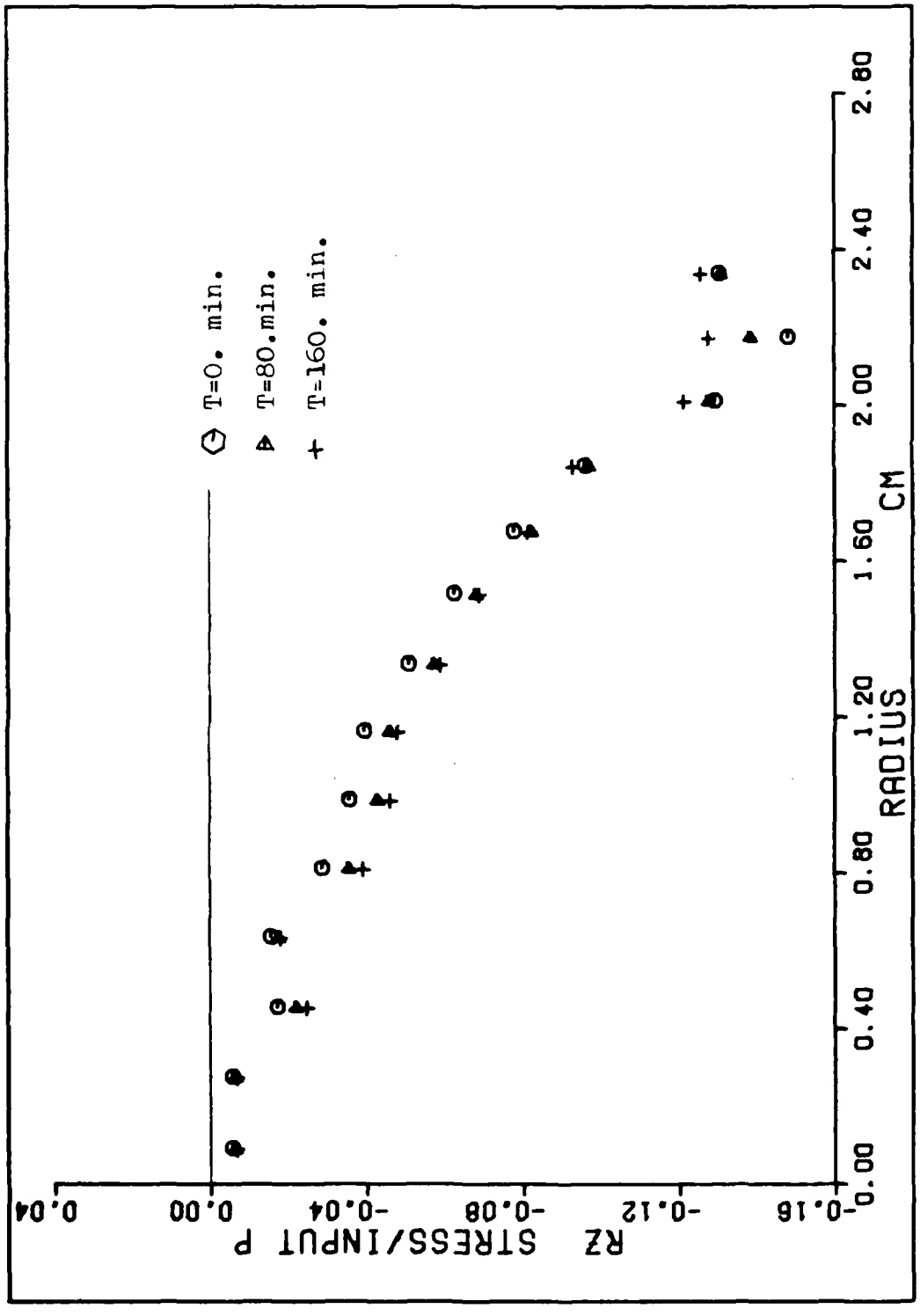

Figure 4.17 RZ Stress/Input P--disc

(σ_{rz})

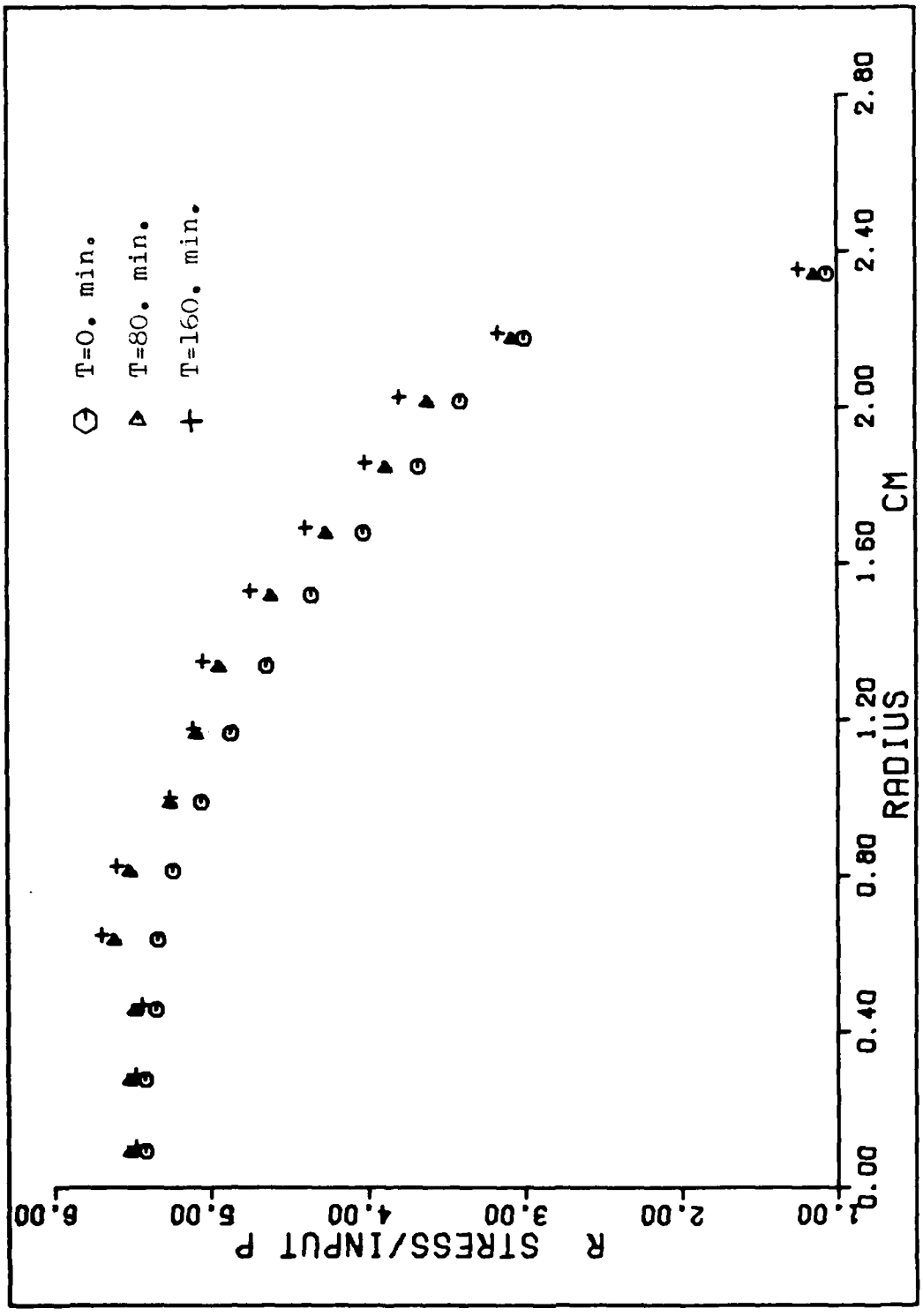

Figure 4.18 R Stress/Input P--Bony End-plate

(σ_r)

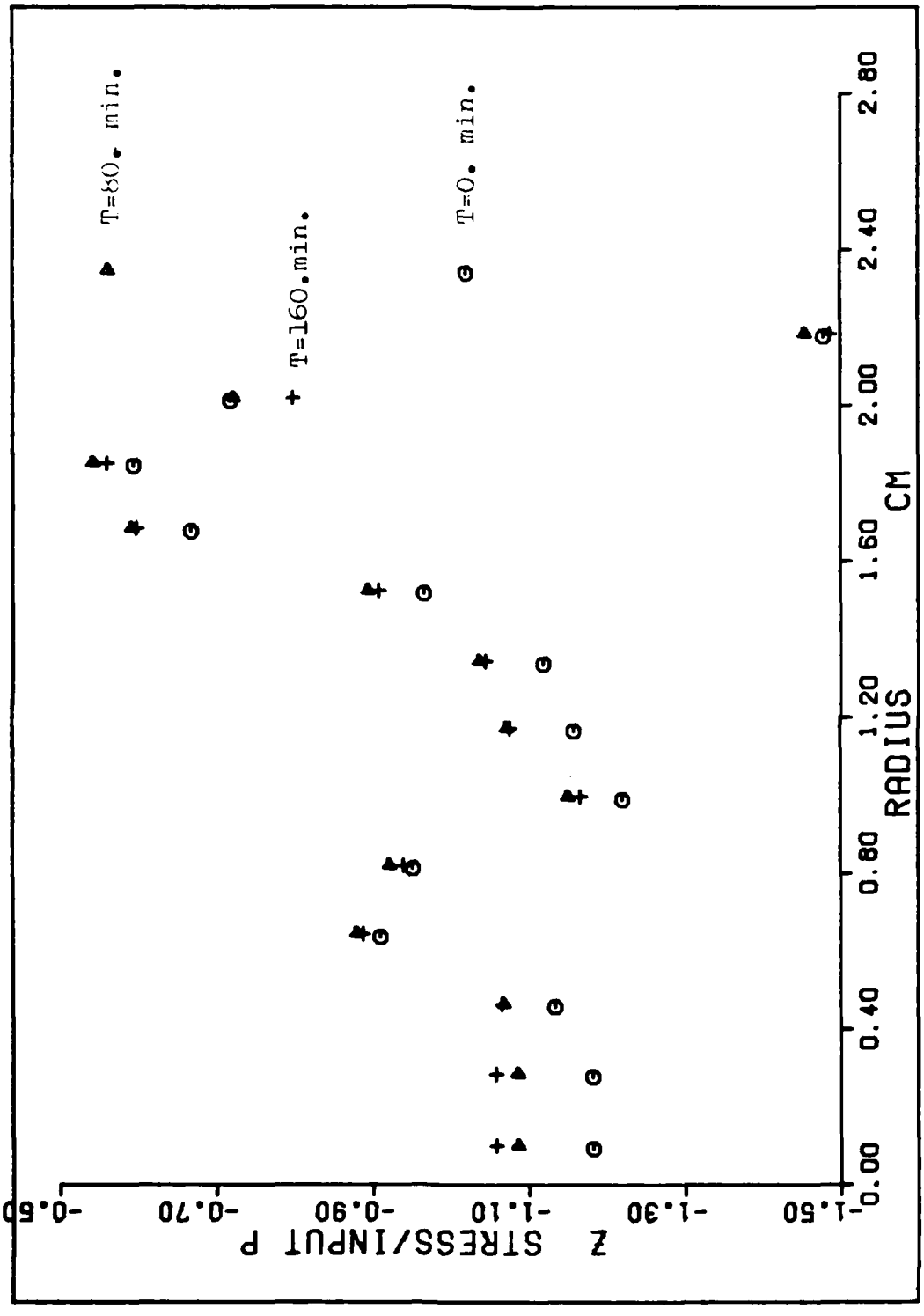

Figure 4.19 Z Stress/Input P--Bony End-plate

(σ_z)

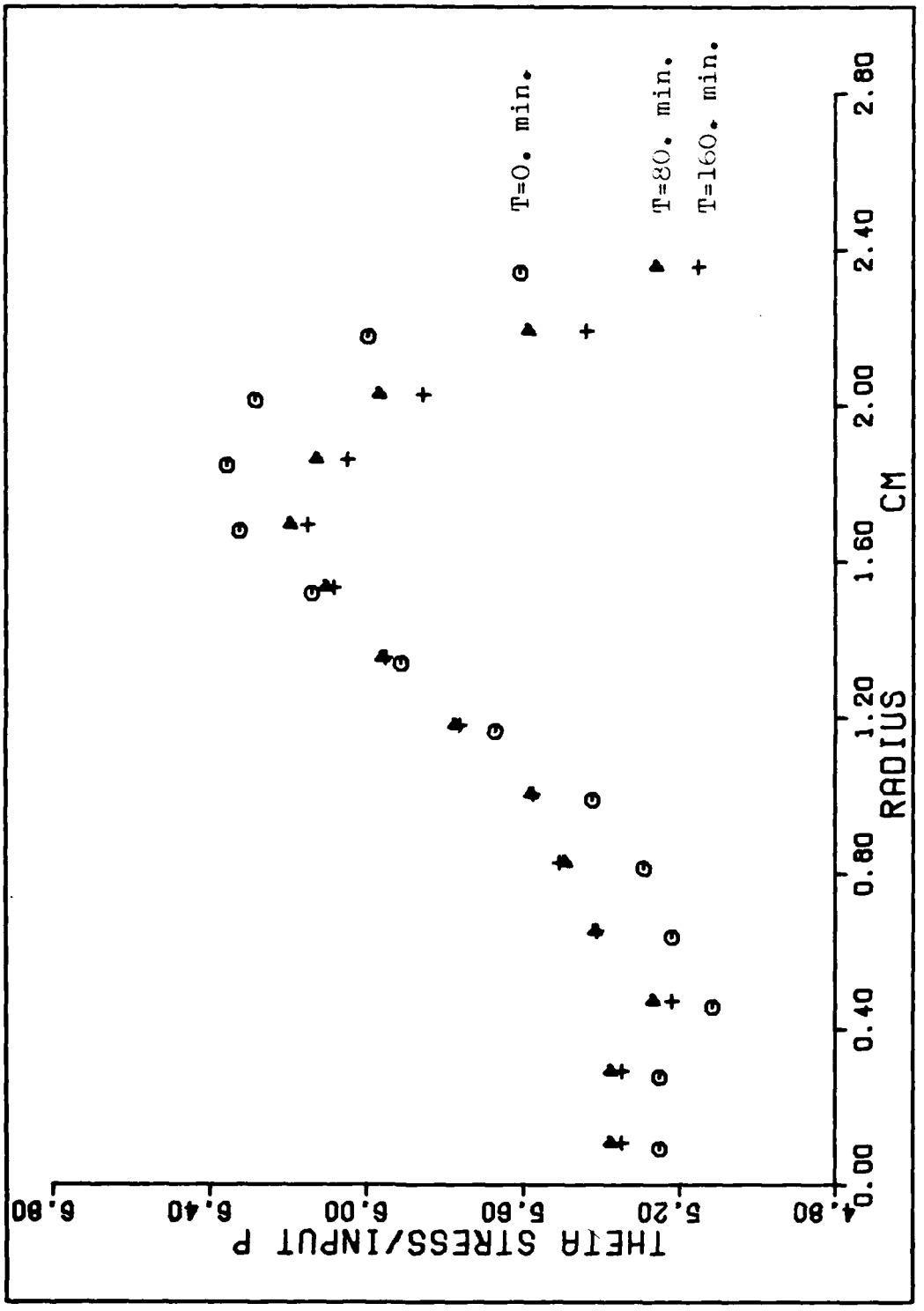

Figure 4.20 Theta Stress/Input P--Bony End-plate

(σ_θ)

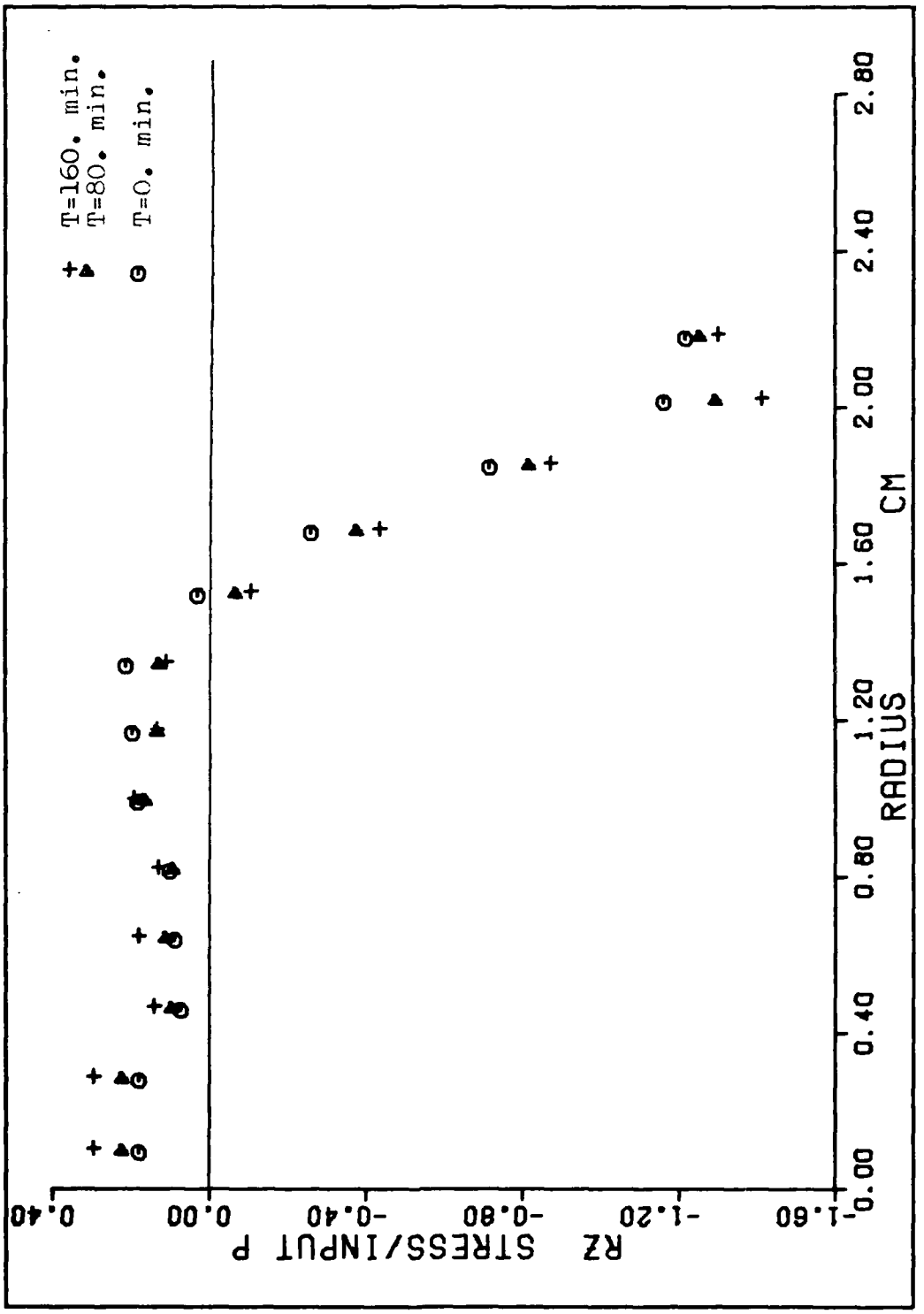

Figure 4.21 RZ Stress/Input P--Bony End-plate

(σ_{rz})

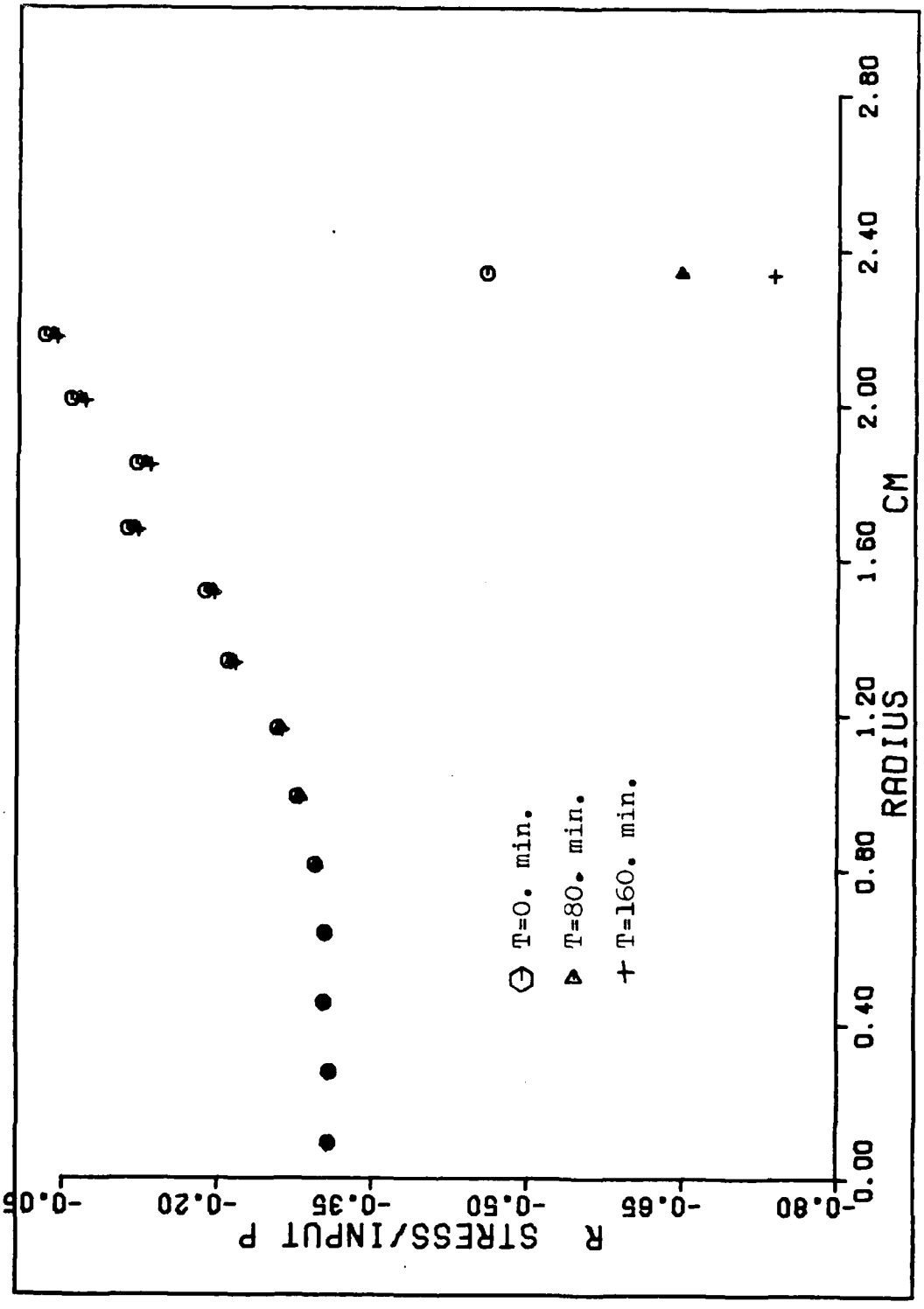

Figure 4.22 R Stress/Input P--Trabecular Bone
(σ_r)

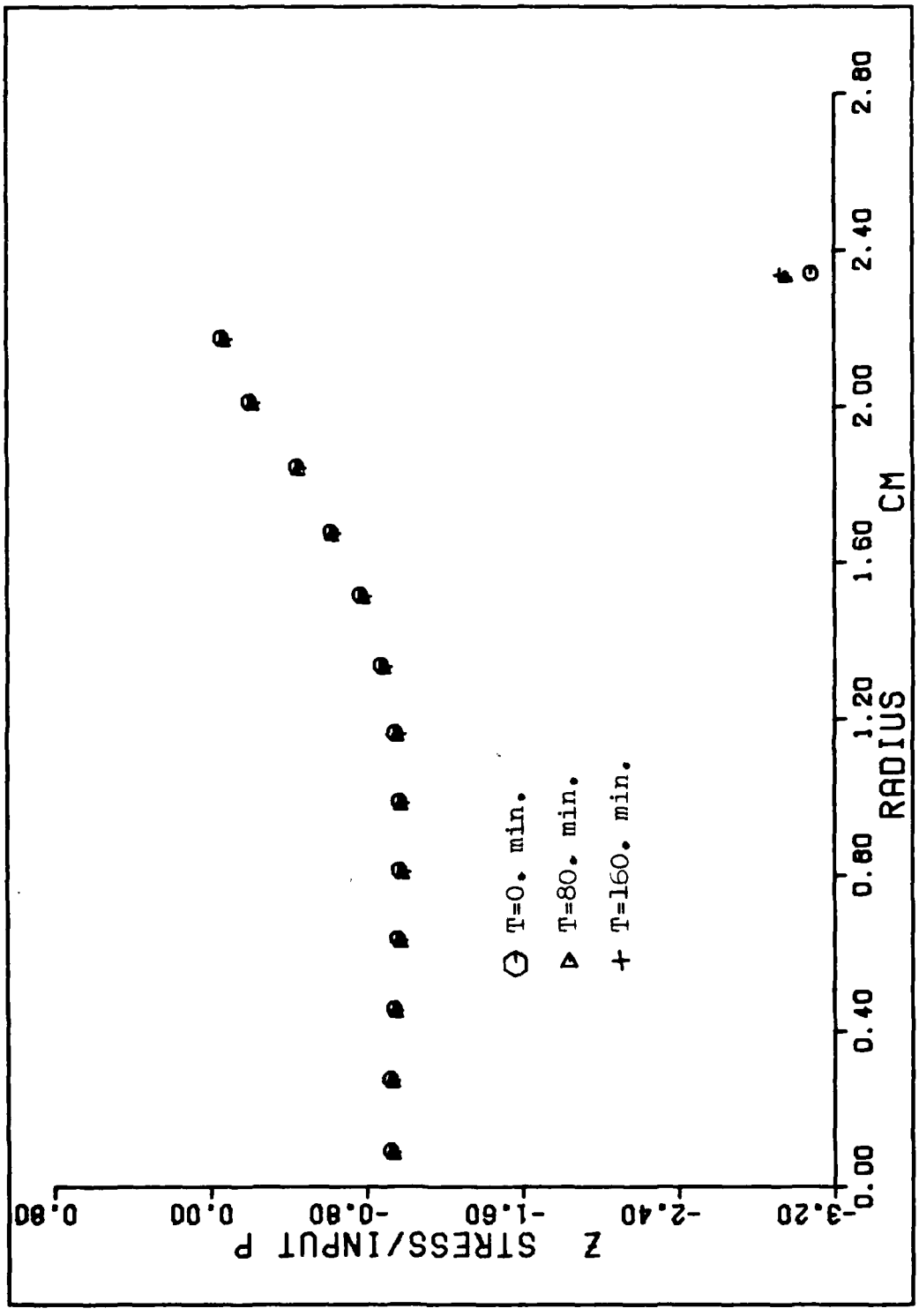

Figure 4.23 Z Stress/Input P--Trabecular Bone
(σ_z)

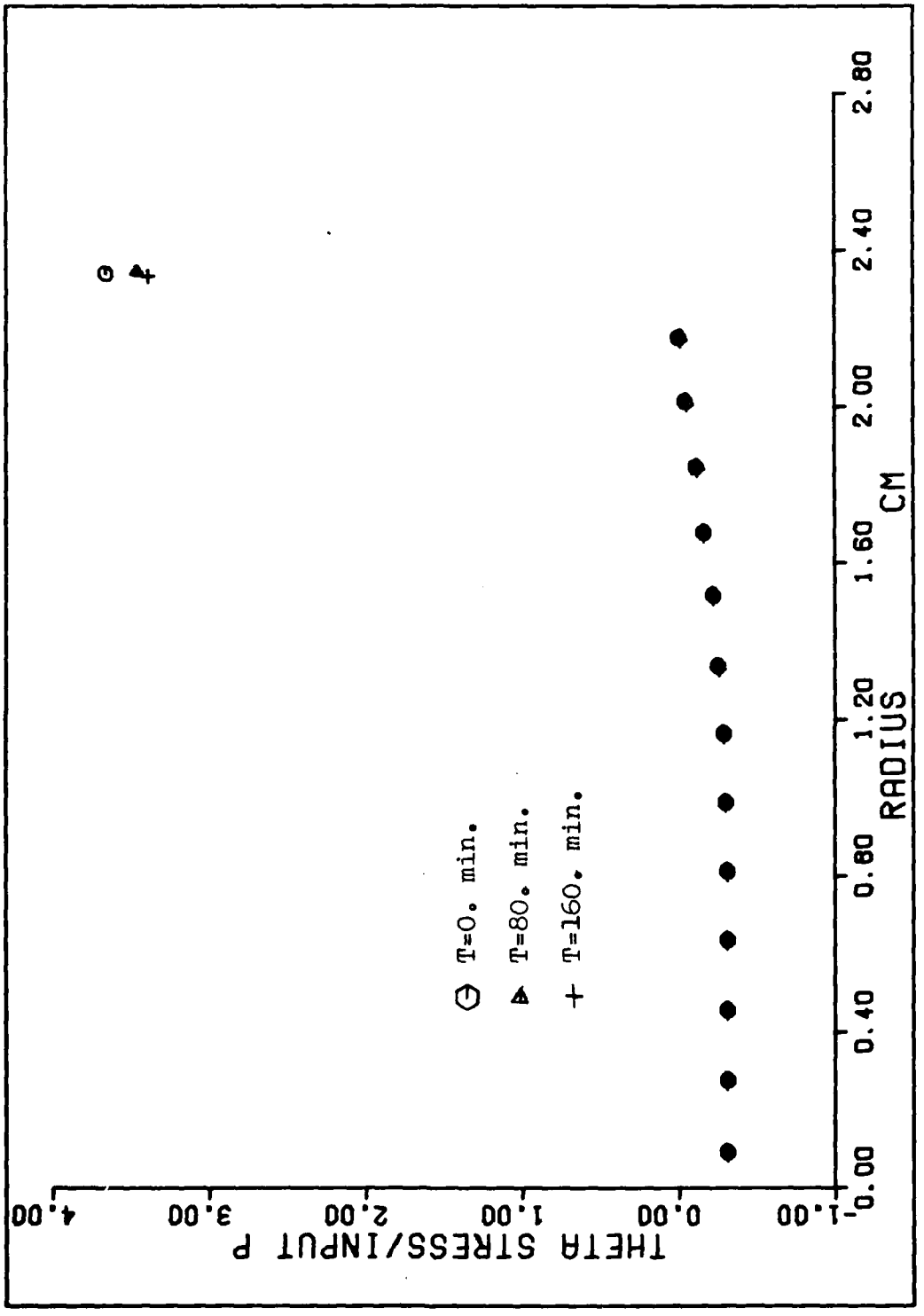

Figure 4.24 Theta Stress/Input P--Trabecular Bone

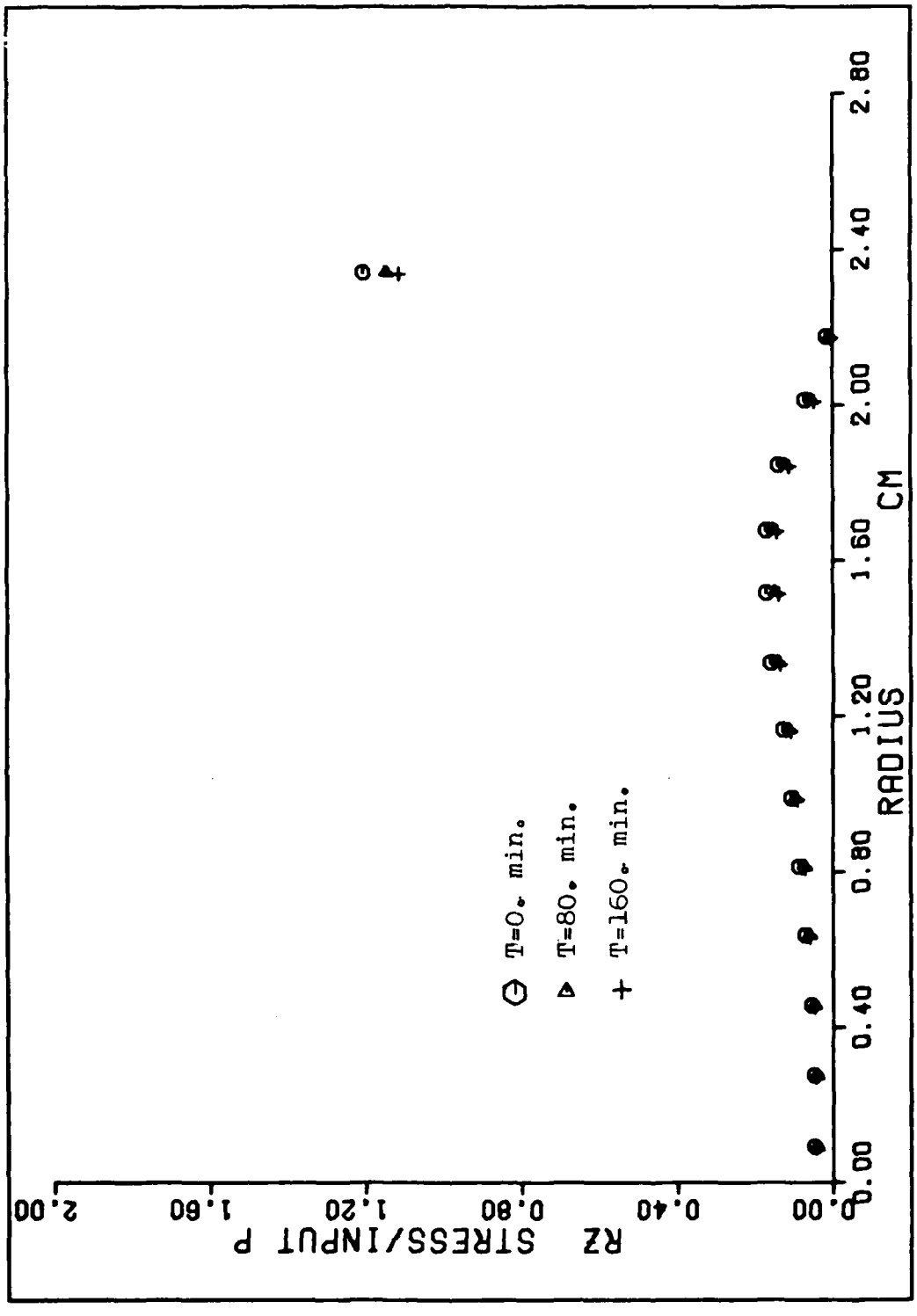

Figure 4.25 RZ Stress/Input P--Trabecular Bone

(γ_{rz})

CHAPTER 5

CONCLUSIONS

Whereas attempts to model the viscoelastic creep of the human intervertebral joint as a one-dimensional viscoelastic structure have proven successful in portraying the externally observed response, they have fallen short of showing the internal response. Furthermore, when attempts are made to apply the viscoelastic parameters derived from such a model to a more complex two-dimensional model, even the external response is not accurately reproduced.

This observation led the author to deviate from the use of the one-dimensionally derived parameters and seek to derive constants which would more accurately reproduce the externally observed response. In doing so, it was found that the material constants based on the axi-symmetric model of the joint varied substantially from those derived from the one-dimensional model. These significant variations led to the conclusion that for purposes of stress analysis, the

one-dimensional parameters are inadequate. Stated alternatively, the intervertebral joint is not accurately modelled as a nonhomogeneous viscoelastic axial rod.

As was pointed out in the preceeding chapter, the viscoelastic creep of the human intervertebral disc causes some significant stress redistributions throughout the entire intervertebral joint. These changes were most pronounced in the disc-bone interface region , where the greatest activity was noted. These redistributions led to the conclusion that time is an important variable which should be included when modelling the human intervertebral joint.

BIBLIOGRAPHY

1. Adey, R.A., Brebbia, C.A., "Efficient Method for Solution of Viscoelastic Problems," Journal of the Engineering Mechanics Division ASCE , Vol 99: 1119-1127, 1973.

2. Balasubramanian, K., Ranu, H.S., King, A.I., "Vertebral Response to Laminectomy," Journal of Biomechanics , Vol 12: 813-823, 1979.

3. Bathe,K-J.,Wilson,E.L., Numerical Methods in Finite Element Analysis , Englewood Cliffs, N.J., Prentice-Hall Inc., 1976.

4. Belytschko,T., Kulak, R.F., Schultz, A.B., and Galante, J.O., "Finte Element Stress Analysis of an Intervertebral Disc," Journal of Biomechanics Vol. 7: 277-285, 1974.

5. Bland, D.R., The Theory of Linear Viscoelasticity , New York, NY, Pergamon Press Inc., 1960.

6. Brown, T., Hansen, R.J. and Yorra, A.J. "Some Mechanical Tests on the Lumbosacral Spine with Particular Reference to the Intervertebral Disc," Journal of Bone and Joint Surgery , Vol. 39A: 1135-1164, 1957.

7. Burns, M.L., "Analytical Modelling of Load Deflection Behavior of Intervertebral Discs Subjected to Axial Compression" , AFOSR-TR-79-0795 , Jul 1979.

8. Christensen, R.M., Theory of Viscoelasticity An Introduction , New York, NY, Academic Press Inc., 1971.

9. Flugge, W., Viscoelasticity , Waltham, Mass., Blaisdell Publishing Co., 1967.

10. Galante, J., Rostaker, W., and Ray, R., "Physical Properties of Trabecular Bone," Calc. Tissue Res. , Vol. 5: 236-246, 1970.

11. Hakim, N.S., King, A.I., "A Three Dimensional Finite Element Dynamic Response Analysis of a Vertebra with Experimental Verification," Journal of Biomechanics , Vol 12: 277-292, 1979.

12. Hinnerichs, T., Viscoplastic and Creep Crack Growth Analysis by the Finite Element Method , Dissertation, Wright Patterson AFB, Oh: Air Force Institute of Technology, June 1980.

13. Hornbeck, R.W., Numerical Methods , New York, NY, Quantum Publishing Inc., 1975.

14. Hirsh,C., "The Reaction of Intervertebral Disc to Compression Forces," Journal of Bone and Joint Surgery ,Vol 37A, 1965.

15. Kazarian, L.E., "Creep Characteristic of the Human Spinal Column," Orthop. Clinics of North America , Vol 6: 1, Jan. 1975.

16. Kazarian, L.E., Kaleps, I., "Mechanical and Physical Properties of the Human Intervertebral Joint," AMRL-TR-79-3 , June 1979.

17. McElhaney, J., Alem, N., and Roberts,V., "A Porous Block Model for Cancellous Bone," ASME Publication Number 70-WA/BHF-2 , 1970.

18. Nachemson, A., "Lumbar Intradiscal Pressure," Acta Orthop. Scand. , Suppl. 43, 1960.

19. Oden, J.T., Finite Elements of Nonlinear Continua , New York, NY, McGraw Hill Book Co. Ltd., 1972.

20. Rockoff, S., Sweet, E. And Bluestein, J., "The Relative Contribution of Trabecular and Cortical Bone to the Strength of Human Lumbar Vertebra," Calc. Tissue Res., Vol. 3: 63-175, 1969.

21. Rolander, S.D., "Motion of the Lumbar Spine with Special Reference to the Stabilizing Effect of Posterior Fusion," Thesis, Acta Orthop. Scand , Suppl. 90, 1966.

22. Saada, A.S., Elasticity , Maxwell House, NY, Pergamon Press Inc., 1974.

23. Spilker, R.L., "A Simplified Finite Element Model of the Intervertebral Disc," International Conference Poceedings Finite Elements in Biomechanics , Vol II : 728-747, 1980.

24. White, J.L., "Finite Elements in Linear Viscoelasticity," AFFDL-TR-68-150 , 1960.

25. Zienkiewicz, O.C., The Finite Element Method 3rd Edition , Maidenhead, Berkshire, England, McGraw-Hill Book Co. Ltd., 1977.

26. Zienkiewicz, O.C., Watson, M., and King, I.P., "A Numerical Method of Viscoelastic Stress Analysis," Int. Journal of Mechanical Science , Vol 10: 807-827, 1968.

APPENDIX A

In the following sections, the basic concepts and equations used in the finite element analysare of elastic materials is briefly reviewed. These equations provide background for the viscoelastic finite element computer program developed. The final section serves to show the incremental nature of the viscoelastic problem and ties the viscoelastic constitutive relation into the elastic solution method.

The basic philosophy of the finite element method (25) is that an approximate solution to a complicated problem can be obtained by subdividing the region of interest into a finite number of discrete elements and then choosing appropriate relatively simple functions to represent the solution within each element. These functions are simple compared to the so-called "exact" solutions which account for the entire region of interest. In this section the equations associated with representing an axisymmetric body as a finite number of elements are presented. The displacements in each element are expressed as a simple polynomial and the equations relating displacements to applied loading are given.

DISPLACEMENT MODEL

The displacement function used in the displacement

formulation is generally selected as a polynomial. The polynomial expression allows for simple differentiation and integration. Also, as the element size becomes small, the polynomial expression permits a simple approximation to the exact solution. A polynomial of infinite order corresponds to an exact solution. However, for practical purposes the polynomial must be truncated to a finite number of terms. Thus, the number of elements in a structure must be large enough so that the displacement function for each element closely approximates the exact displacements in that particular region.

In any numerical method, the solution should converge to the exact solution as the size of the elements become small. For the displacement formulation, it has been shown that under certain conditions the solution provides a lower bound to the exact displacements (25). To assure this convergence certain conditions must be satisfied. First, the displacement function must be chosen so that rigid body displacements do not cause straining of the element. Second, the function must also be chosen so that a constant state of strain is obtained as the element size approaches zero. The simplest polynomial function which satisfies these two requirements and also maintains displacement continuity between adjacent elements is the linear displacement function.

DISPLACEMENT FUNCTION

Figure A-1 shows a typical triangular element, m, with nodes i,j,k numbered in a counter clockwise direction. The linear displacement function which defines the displacements within the element is given by

$$u = \alpha_1 + \alpha_2 r + \alpha_3 z$$
$$v = \alpha_4 + \alpha_5 r + \alpha_6 z \qquad \text{(A-1)}$$

where the constants α_i are determined from the six nodal displacements and nodal coordinates as

$$\begin{Bmatrix} \alpha_1 \\ \alpha_2 \\ \alpha_3 \end{Bmatrix} = \frac{1}{2A_m} \begin{bmatrix} a_i & a_j & a_k \\ b_i & b_j & b_k \\ c_i & c_j & c_k \end{bmatrix} \begin{Bmatrix} u_i \\ u_j \\ u_k \end{Bmatrix} \qquad \text{(A-2)}$$

and

$$\begin{Bmatrix} \alpha_4 \\ \alpha_5 \\ \alpha_6 \end{Bmatrix} = \frac{1}{2A_m} \begin{bmatrix} a_i & a_j & a_k \\ b_i & b_j & b_k \\ c_i & c_j & c_k \end{bmatrix} \begin{Bmatrix} v_i \\ v_j \\ v_k \end{Bmatrix} \qquad \text{(A-3)}$$

where A_m is the in-plane area of the element. The coefficients a_i, b_i, and c_i are given by

$$a_i = r_j z_k - r_k z_j \qquad \text{(A-4)}$$

$$b_i = z_j - z_k \qquad \text{(A-5)}$$

$$c_i = r_k - r_j \qquad \text{(A-6)}$$

where r and z are coordinates of the nodal points. The other coefficients for the subscripts "j" and "k" are obtained by cyclic permutation of the subscripts i, j, and k.

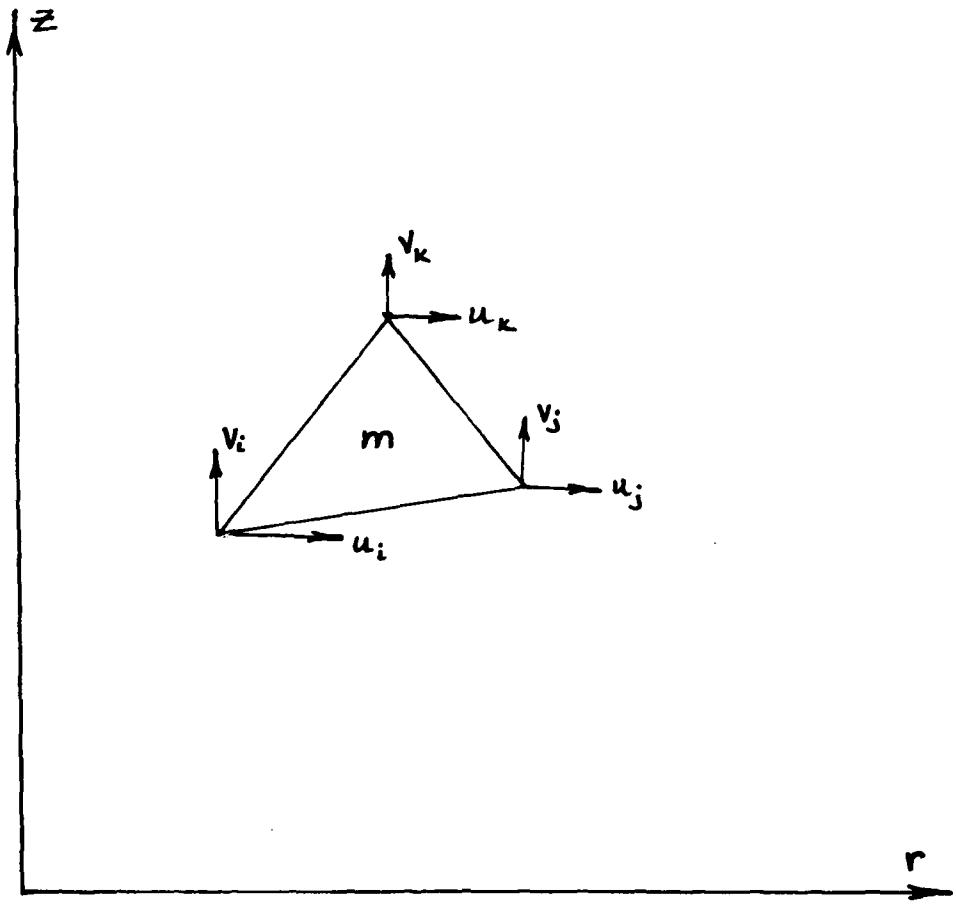

Figure A-1 Typical Triangular Element

AD-A094 774 AIR FORCE INST OF TECH WRIGHT-PATTERSON AFB OH SCHOO--ETC F/G 6/16
A VISCOELASTIC FINITE ELEMENT MODEL OF THE HUMAN INTERVERTEBRAL--ETC(U)
DEC 80 R L HINRICHSEN
UNCLASSIFIED AFIT/GAE/AA/80D-11 NL

2 OF 2
AD A094774

END
DATE FILMED
8-81
DTIC

ELEMENT STRAIN FOR AN AXI-SYMMETRIC GEOMETRY

The total strains at any point within an element are defined in terms of the displacement derivatives as

$$\{\epsilon\} = \begin{Bmatrix} \epsilon_z \\ \epsilon_r \\ \epsilon_\theta \\ \gamma_{rz} \end{Bmatrix} = \begin{Bmatrix} \partial v/\partial z \\ \partial u/\partial r \\ u/r \\ \partial u/\partial z + \partial v/\partial r \end{Bmatrix} \qquad \text{(A-7)}$$

From eqs A-1 to A-6, the total strains are written in terms of the nodal displacements and coordinates as

$$\{\epsilon\} = [B]\{u\} \qquad \text{(A-8)}$$

where $\{u\}$ is the generalized nodal displacement and

$$[B] = \frac{1}{2A_m} \begin{bmatrix} 0 & c_i & 0 & c_j & 0 & c_k \\ b_i & 0 & b_j & 0 & b_k & 0 \\ \gamma_i & 0 & \gamma_j & 0 & \gamma_k & 0 \\ c_i & b_i & c_j & b_j & c_k & b_k \end{bmatrix} \qquad \text{(A-9)}$$

where

$$\gamma_i = a_i/r + b_i + c_i z/r$$

ELASTIC ANALYSIS

For linear elastic and isotropic materials, the relationship between stresses $\{\sigma\}$, strains $\{\epsilon\}$ and any initial strains $\{\epsilon_o\}$ is given by

$$\{\sigma\} = \begin{Bmatrix} \sigma_z \\ \sigma_r \\ \sigma_\theta \\ \tau_{rz} \end{Bmatrix} = [D]\{\{\epsilon\} - \{\epsilon_o\}\} \qquad \text{(A-10)}$$

where [D] is the elastic material property matrix. The

matrix [D] for axisymmetric conditions is given by

$$[D] = \frac{E(1-\nu)}{(1+\nu)(1-2\nu)} \begin{bmatrix} 1 & \nu/1-\nu & \nu/1-\nu & 0 \\ & 1 & \nu/1-\nu & 0 \\ & \text{Sym} & 1 & 0 \\ & & & \frac{1-2\nu}{2(1-\nu)} \end{bmatrix} \quad \text{(A-11)}$$

METHOD of SOLUTION

The equation which governs the elastic response of a discretized structure can be derived from the principle of virtual work (25) and is given by

$$[K]\{u\} = \{P\} + \{Q\} \quad \text{(A-12)}$$

where [K] is the elastic stiffness matrix of the structure $\{u\}$ is the generalized displacement vector, $\{P\}$ is the external applied load vector, and $\{Q\}$ is the force vector due to the presence of initial strain.

The coefficients of the elastic stiffness matrix are obtained from

$$[K] = \sum_{M=1}^{M} 2\pi \int [B]^T [D] [B] \, r \, dr \, dz \quad \text{(A-13)}$$

where the integration is taken over the volume of each element and the summation is over all elements in the structure. The nodal forces due to initial strains are given by

$$\{Q\} = \sum_{M=1}^{M} \int [B]^T [D] \{\epsilon_0\} \, dV_0 \quad \text{(A-14)}$$

Since the integrals contain terms which are dependant on the radius r, an efficient method of integration must be chosen. The simplest approximation procedure is to evaluate $[\beta]$ for a centroidal point

$$\bar{r} = (r_i + r_j + r_k)/3 \qquad \text{(A-15)}$$

$$\bar{z} = (z_i + z_j + z_k)/3 \qquad \text{(A-16)}$$

In this case, if $[\bar{\beta}]$ is defined to be $[\beta]$ evaluated at the centroidal point

$$[K] = \sum_{m=1}^{M} 2\pi A_m [\bar{B}]^T [D][\bar{B}]\,\bar{r} \qquad \text{(A-17)}$$

$$\{Q\} = \sum_{m=1}^{M} 2\pi A_m [\bar{B}]\,[D]\{\epsilon_0\}\,\bar{r} \qquad \text{(A-18)}$$

In the elastic problem, the unknowns are the displacements $\{u\}$. The solution for these unknowns is found by the inversion of Eqn A-12.

VISCOELASTIC PROBLEMS

As discussed in Chapter 3, the displacements, strains,

and stresses are seen to be time dependant in viscoelastic problems. It is also seen that the constitutive relation for a three-parameter solid can be integrated in time to give Eqn 2-50 which repeated here is

$$\{\Delta\epsilon_c\} = \frac{\Delta t}{q_1}\left[\tfrac{2}{3}[A]\{\sigma\} - q_0\{\epsilon_c\}\right] \qquad \text{(A-19)}$$

where [A] is given by

$$[A] = \begin{bmatrix} 1 & -\nu_e & -\nu_e & 0 \\ & 1 & -\nu_e & 0 \\ & & 1 & 0 \\ \text{Sym} & & & \frac{1-\nu_e}{2} \end{bmatrix} \qquad \text{(A-20)}$$

If $\{\Delta\epsilon_c\}$ is treated as an incremental initial strain $\{\epsilon_0\}$, then it is readily seen that the viscoelastic constitutive relation enters into the governing equation (A-12) only in the residual force term $\{Q\}$. Then, as time is incremented by imposing a small Δt, the residual force term is seen to vary with time. This means that Eqn A-12 must be solved at each time step for the values of

$$\{u\}\ ,\ \{\epsilon\} = \{\epsilon_e\} + \{\epsilon_c\}\ ,\ \{\sigma\} \qquad \text{(A-21)}$$

These values of $\{\sigma\}$ and $\{\epsilon_c\}$ are then substituted in to Eqn A-19 , time is incremented, and the process continues until a maximum time is reached. Figure A-2 presents a flow chart of the procedure.

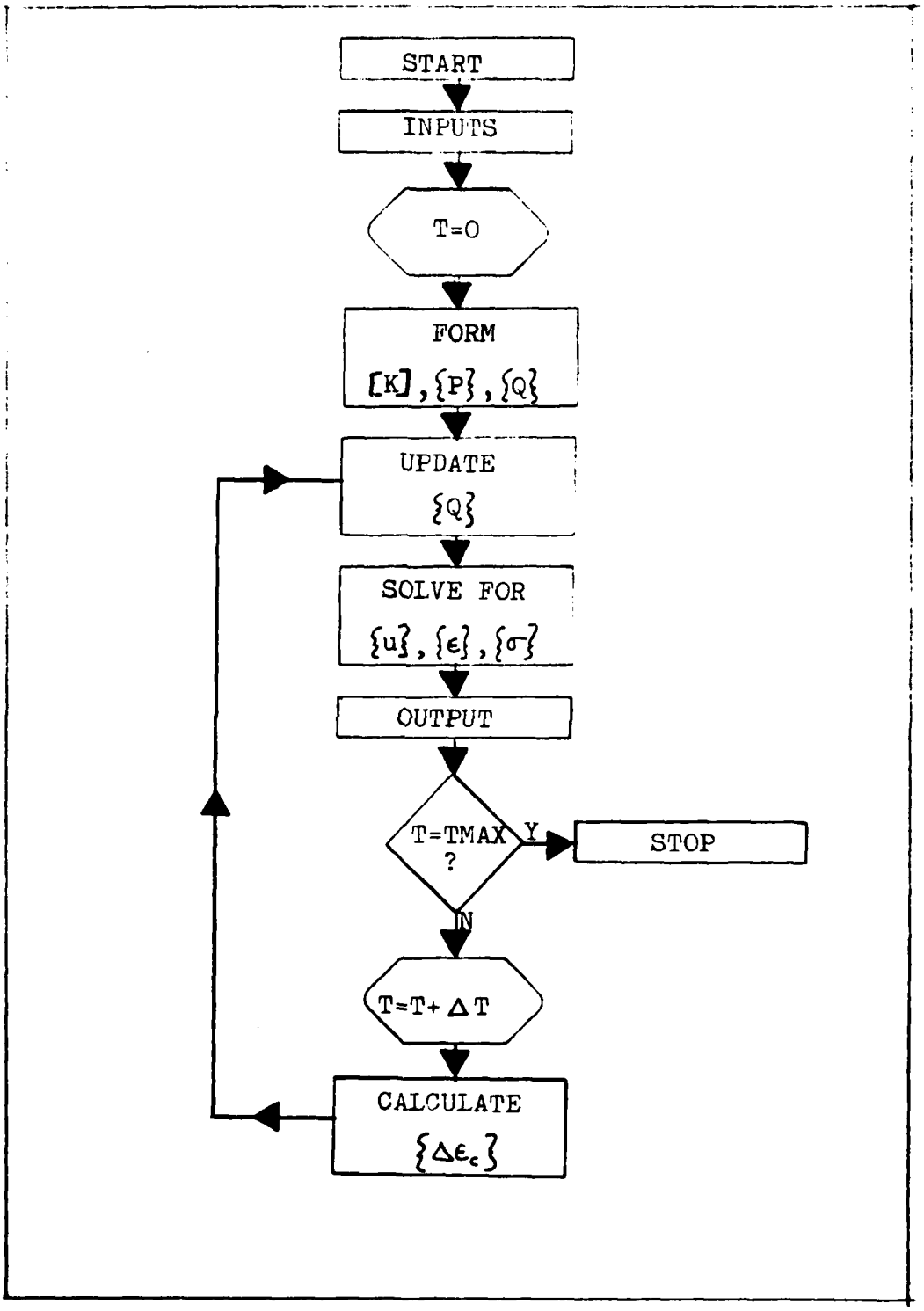

Figure A-2 Flow Chart of Solution Technique

APPENDIX B

The application of the general correspondence principle to obtain the viscoelastic solution to the thick-walled cylinder problem proceeds as follows:

$$\bar{u}_r = \frac{\bar{p}\,b^2}{a^2-b^2}\,\frac{Q'}{2'}\left[\frac{3\,2'Q''}{2Q'2''+2'Q''}\,r + \frac{a^2}{r}\right] \qquad \text{(B-1)}$$

Applying the assumption that the volume change is purely elastic, while the distortion is a three-parameter solid, leads to the following operators:

$$Q'' = 1\ ;\quad 2'' = 3K\ ;\quad Q' = 1+p_1\Delta\ ;\quad 2' = q_0+q_1\Delta \qquad \text{(B-2)}$$

Substituting into Eqn B-1 yields

$$\bar{u}_r = \frac{\bar{p}\,b^2}{a^2-b^2}\left(\frac{1+p_1\Delta}{q_0+q_1\Delta}\right)\left[\frac{3(q_0+q_1\Delta)}{6K(1+p_1\Delta)+(q_0+q_1\Delta)}\,r + \frac{a^2}{r}\right] \qquad \text{(B-3)}$$

$$\bar{u}_r = \frac{\bar{p}\,b^2}{a^2-b^2}\left[\frac{3(1+p_1\Delta)}{6K+6Kp_1\Delta+q_0+q_1\Delta}\,r + \frac{a^2(1+p_1\Delta)}{r(q_0+q_1\Delta)}\right] \qquad \text{(B-4)}$$

$$\bar{u}_r = \frac{\bar{p}\,b^2}{a^2-b^2}\left[\frac{3r+3p_1r\Delta}{6K+6Kp_1\Delta+q_0+q_1\Delta} + \frac{a^2+p_1a^2\Delta}{q_0r+q_1r\Delta}\right] \qquad \text{(B-5)}$$

$$\bar{u}_r = \frac{\bar{p}\,b^2}{a^2-b^2}\left[\frac{3r+3p_1 r s}{(6K+q_0)+(6Kp_1+q_1)s} + \frac{a^2+p_1 a^2 s}{q_0 r + q_1 r s}\right] \quad \text{(B-6)}$$

$$\bar{u}_r = \frac{\bar{p}\,b^2}{a^2-b^2}\left[\frac{3r}{(6K+q_0)+(6Kp_1+q_1)s} + \frac{3p_1 r s}{(6K+q_0)+(6Kp_1+q_1)s}\right. \quad \text{(B-7)}$$

$$\left. + \frac{a^2}{q_0 r + q_1 r s} + \frac{p_1 a^2 s}{q_0 r + q_1 r s}\right]$$

At this point, the method of load application must be considered. If the load is applied instantaneously, the value of $\bar{p}$ becomes $p=p/s$. Substituting and rearranging leads to

$$\bar{u}_r = \frac{p\,b^2}{a^2-b^2}\left\{\frac{3r}{6Kp_1+q_1}\left[\frac{1}{s\left(\frac{6K+q_0}{6Kp_1+q_1}+s\right)}\right] + \frac{3rp_1}{6Kp_1+q_1}\left[\frac{1}{\left(\frac{6K+q_0}{6Kp_1+q_1}+s\right)}\right]\right. \quad \text{(B-8)}$$

$$\left. + \frac{a^2}{q_1 r}\left[\frac{1}{s(q_0/q_1+s)}\right] + \frac{p_1 a^2}{q_1 r}\left[\frac{1}{(q_0/q_1+s)}\right]\right\}$$

The equation in this form is conveniently inverted to the time domain by the following expressions:

$$\frac{1}{a+s} \longrightarrow e^{-at} \quad \text{(B-9)}$$

and

$$\frac{1}{s(a+s)} \longrightarrow \frac{1}{a}\left(1-e^{-at}\right) \quad \text{(B-10)}$$

so

$$u_r = \frac{pb^2}{a^2-b^2}\left\{\frac{3r}{6K+q_0}\left[1-e^{-\alpha t}\right] + \frac{3rp_1}{6Kp_1+q_1}\,e^{-\alpha t}\right.$$
$$\left. + \frac{a^2}{q_0 r}\left[1-e^{-\beta t}\right] + \frac{p_1 a^2}{q_1 r}\,e^{-\beta t}\right\} \qquad \text{(B-11)}$$

where $\alpha = \dfrac{6K+q_0}{6Kp_1+q_1}$; $\beta = q_0/q_1$

To obtain the value of σ_z, consider the transformed equation

$$\bar{\sigma}_z = \frac{2\bar{p}b^2}{a^2-b^2}\left[\frac{\Theta' Z'' - Z'\Theta''}{2\Theta' Z'' + Z'\Theta''}\right] \qquad \text{(B-12)}$$

Substituting in the polynomial operators from Eqn B-2 yields

$$\bar{\sigma}_z = \frac{2\bar{p}b^2}{a^2-b^2}\left[\frac{(1+p_1\Delta)3K - q_0 - q_1\Delta}{6K(1+p_1\Delta) + q_0 + q_1\Delta}\right] \qquad \text{(B-13)}$$

$$\bar{\sigma}_z = \frac{2\bar{p}b^2}{a^2-b^2}\left[\frac{(3K-q_0)+(3Kp_1-q_1)\Delta}{(6K+q_0)+(6Kp_1+q_1)\Delta}\right] \qquad \text{(B-14)}$$

Again assuming instantaneous loading leads to

$$\bar{\sigma}_z = \frac{2pb^2}{a^2-b^2}\left\{\frac{3K-q_0}{6Kp_1+q_1}\left[\frac{1}{\Delta\left(\frac{6K+q_1}{6Kp_1+q_1}+\Delta\right)}\right] + \frac{3Kp_1-q_1}{6Kp_1+q_1}\left[\frac{1}{\frac{6K+q_0}{6Kp_1+q_1}+\Delta}\right]\right\} \qquad \text{(B-15)}$$

Using the same inversion expressions gives

$$\sigma_z = \frac{2pb^2}{a^2-b^2}\left\{\frac{3K-q_0}{6K+q_0}\left[1-e^{-\alpha t}\right] + \frac{3Kp_1-q_1}{6Kp_1+q_1}\,e^{-\alpha t}\right\} \qquad \text{(B-16)}$$

where, again

$$\alpha = \frac{6K+q_0}{6Kp_1+q_1}$$

VITA

Ronald L Hinrichsen was born on 6 June 1949 at Great Falls, Montana. He graduated from C.M. Russell High School in Great Falls in 1967. He enlisted in the Air Force in 1969 and worked as a Minuteman Missile Mechanic at Ellsworth AFB, South Dakota. In June 1973, he was accepted into the Airman Education and Commissioning Program, and attended the University of Arizona in Tucson, where he graduated with high distinction with a B.S. in Aeronautical Engineering in 1975. Following attendance at Officer Training School at Lackland AFB, Texas, he was stationed at Lowry AFB, Colorado where he served as a data analyst for the Foreign Technology Division. In June 1979 he came to the Air Force Institute of Technology to pursue a M.S. Degree in Aerospace Engineering. He is currently being extended into the PhD program at AFIT.

He married Miss Kay Lynn Smith in 1967 and they have six children Peter, Renae, Kristen, Ronald, Jarrod, and Heather.

Unclassified

SECURITY CLASSIFICATION OF THIS PAGE *(When Data Entered)*

REPORT DOCUMENTATION PAGE		READ INSTRUCTIONS BEFORE COMPLETING FORM
1. REPORT NUMBER AFIT/GAE/AA/80D-11	2. GOVT ACCESSION NO. AD-A094774	3. RECIPIENT'S CATALOG NUMBER
4. TITLE *(and Subtitle)* A VISCOELASTIC FINITE ELEMENT MODEL OF THE HUMAN INTERVERTEBRAL JOINT		5. TYPE OF REPORT & PERIOD COVERED MS THESIS
		6. PERFORMING ORG. REPORT NUMBER
7. AUTHOR(s) Ronald L. Hinrichsen Captain		8. CONTRACT OR GRANT NUMBER(s)
9. PERFORMING ORGANIZATION NAME AND ADDRESS Air Force Institute of Technology (AFIT-EN) Wright-Patterson AFB, Ohio 45433		10. PROGRAM ELEMENT, PROJECT, TASK AREA & WORK UNIT NUMBERS
11. CONTROLLING OFFICE NAME AND ADDRESS		12. REPORT DATE December 1980
		13. NUMBER OF PAGES 105
14. MONITORING AGENCY NAME & ADDRESS*(if different from Controlling Office)*		15. SECURITY CLASS. *(of this report)* Unclassified
		15a. DECLASSIFICATION DOWNGRADING SCHEDULE

16. DISTRIBUTION STATEMENT *(of this Report)*

Approved for public release; distribution unlimited

17. DISTRIBUTION STATEMENT *(of the abstract entered in Block 20, if different from Report)*

18. SUPPLEMENTARY NOTES

Approved for public release; IAW AFR 190-17

Frederic C. Lynch, Major, USAF
Director of Public Affairs

30 DEC 1980

19. KEY WORDS *(Continue on reverse side if necessary and identify by block number)*

Viscoelastic
Finite Element
Intervertebral Joint

20. ABSTRACT *(Continue on reverse side if necessary and identify by block number)*

The combined mechanical stresses on aircrewmen have become increasingly acute as technological developments extend the flight envelopes of our high performance aircraft. Limitations on the design of this type of aircraft are frequently dictated by human tolerance. The concept of an analytical model to evaluate the biomechanical response of the human intervertebral joint, under the

DD FORM 1 JAN 73 1473 EDITION OF 1 NOV 65 IS OBSOLETE

Unclassified

SECURITY CLASSIFICATION OF THIS PAGE *(When Data Entered)*

influence of long term axial compressive loading, is important in assessing the load carrying capability of normal and diseased vertebral segments.

It has been experimentally demonstrated that healthy intervertebral joints are composed of materials which exhibit creep characteristics. This investigation is significant because it presents a study of the time dependant behavior involved. An axisymmetric finite element model is employed which incorporates a linear viscoelastic constitutive relation for the intervertebral disc. Viscoelastic material constants are found by matching one-dimensional data with the two-dimensional model. Results are presented depicting displacement profiles and stress redistributions occurring as a consequence of the inclusion of these viscoelastic parameters which, for the first time, simulate the actual human response to high compressive loads over a specific time span.

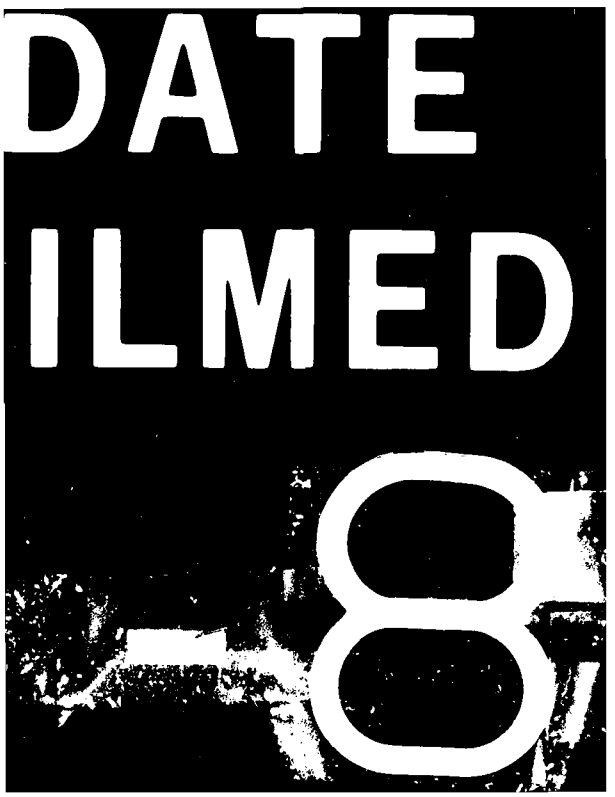
DATE
ILMED